Atmósfera 40, 1-34 (2026)
https://doi.org/10.20937/ATM.53471

Impact of climate variability on land use and groundwater resources: A case study of Wadi Fekan, northwest Algeria

Abdelkader OUIKHLEF[1,3]*, Abdelkader OTMANE[2,3], Radia GHERISSI[1,3] and Mohamed El-Amine GACEMI[4,5]

[1] *Department of Hydraulics, Institute of Science and Technology, University Centre of Maghnia, 13300 Tlemcen, Algeria.*
[2] *Faculty of Natural Sciences and Life, Ibn Khaldoun Tiaret University, Karman, BP14000, Tiaret, Algeria*
[3] *Laboratory No 25, Promotion of the Water Resources, Mines, and Pedological, Legislation of the Environment and Technological Choices, University of Tlemcen, 13300 Tlemcen, Algeria*
[4] *Centre des Techniques Spatiales, 01 avenue de la Palestine BP 13,31200 Arzew, Algeria.*
[5] *University of Oran 2-Mohamed Ben Ahmed, Oran, Algeria.*
*Corresponding author; email: a.ouikhlef@cu-maghnia.dz

Received: February 12, 2025; Accepted: October 16, 2025

RESUMEN

La región mediterránea es altamente vulnerable a la variabilidad climática, con profundas implicaciones para la seguridad hídrica. Este estudio evalúa el impacto de cuatro décadas (1983-2023) de fluctuaciones climáticas sobre el uso del suelo y los recursos de agua subterránea en la subcuenca de Wadi Fekan, en el noroeste de Argelia. Mediante el uso de índices estandarizados (SPI, CMI) y pruebas de detección de rupturas aplicadas a los datos de 11 estaciones pluviométricas, se identificó un cambio climático clave entre 1999 y 2006. Esta ruptura marcó el inicio de un régimen más húmedo, con un aumento del 31.7 % en las precipitaciones. El incremento resultante del escurrimiento provocó una expansión medible del cauce principal del río (+0.045 % en la clase de uso del suelo). Paralelamente, el acuífero aluvial experimentó una recarga significativa, con volúmenes que aumentaron de 17.997 km^3 (2003-2013) a 25.615 km^3 (2013-2023). No obstante, el análisis espacial reveló una paradoja: a pesar de las condiciones más húmedas en general, la aridez se intensificó en el centro de la cuenca debido a un efecto Foehn, y el balance hídrico neto del acuífero se mantuvo negativo durante todo el periodo de estudio. Esto indica que la sobreexplotación del agua subterránea durante las sequías anteriores generó un déficit hidrológico que las precipitaciones recientes no han compensado por completo. Estos resultados demuestran la persistente vulnerabilidad de los acuíferos semiáridos frente al estrés climático y la presión antrópica, subrayando la necesidad crítica de estrategias de gestión sostenible que aborden tanto la variabilidad climática como la sobreexplotación histórica para mitigar futuras crisis hídricas.

ABSTRACT

The Mediterranean region is highly vulnerable to climate variability, with profound implications for water security. This study assesses the impact of four decades (1983-2023) of climatic fluctuations on land use and groundwater resources in the Wadi Fekan sub-watershed, northwest Algeria. Using standardized indices (SPI, CMI) and break detection tests on data from 11 rainfall stations, we identified a pivotal climatic shift between 1999 and 2006. This break initiated a wetter regime, leading to a 31.7% increase in rainfall. The resulting increase in runoff led to a measurable expansion of the main riverbed (+0.045% in land-use class). Concurrently, the alluvial aquifer experienced substantial recharge, with volumes rising from 17.997 km^3 (2003-2013) to 25.615 km^3 (2013-2023). However, spatial analysis revealed a paradox: despite overall wetter conditions, aridity intensified in the basin's center due to a Foehn effect, and the aquifer's net water balance remained negative over the study period. This indicates that groundwater overexploitation during prior droughts created a hydrologic deficit that recent rainfall has not fully offset. These findings demonstrate the persistent vulnerability of semi-arid aquifers to climatic stress and anthropogenic pressure, underscoring the critical need for sustainable management strategies that address both climate variability and historical overuse to mitigate future water crises.

Keywords: Algeria, Fekan, climatic fluctuations, drought, groundwater resources, land use.

1. Introduction

This study investigates the interrelated impacts of climate variability on groundwater resources and land-use dynamics in the semi-arid Oued Fekan watershed in northwestern Algeria. Understanding these coupled processes is crucial for designing sustainable adaptation strategies in Mediterranean environments increasingly exposed to climate change. While previous studies have often examined climate impacts on water and land systems in isolation, this research adopts an integrated approach to analyze their simultaneous evolution and interactions.

Climate change stems from both natural processes within the climate system—such as ocean circulation and solar cycle variations—and external factors, including volcanic activity and anthropogenic influences such as fossil fuel combustion and land-use modification (CSEN, 2022). According to the Intergovernmental Panel on Climate Change (IPCC, 2007), projections indicate a temperature rise of 2-3 ºC in the Mediterranean region by 2050 and 3-5 ºC by 2100. These increases are expected to reduce relative humidity, enhance atmospheric moisture capacity, and alter precipitation patterns, leading to less frequent but more intense rainfall events and extended drought periods (Milano, 2010).

Recent decades have witnessed a global escalation of extreme weather events, including floods, droughts, and desertification, prompting growing scientific concern (Jouilil et al., 2013; Soro et al., 2014; Faye et al., 2015; Faty et al., 2017; Otmane et al., 2018; Jaziri et al., 2019). Research on drought evolution highlights the current period as one of the longest and most severe on record (Paturel et al., 1998; Eriksen and Kelly, 2007; Dao et al., 2010; Aicha et al., 2011; Hallouz et al., 2012; Ghenim, 2013; Khoualdia et al., 2014; Kartoubi et al., 2017; Amiar et al., 2020; Bekkoussa, 2020). This phenomenon remains poorly understood due to its pronounced spatial heterogeneity and temporal variability, particularly across Africa (Bessedik et al., 2023).

In this context, groundwater is a vital resource in arid and semi-arid regions. Assessing its renewal capacity is essential for ensuring the sustainability of this increasingly scarce resource (Issartel, 2007), making the understanding of drought impacts on aquifers fundamental for effective long-term management.

The Oued Fekan watershed, situated in one of Algeria's key agricultural areas, benefits from a favorable hydrogeological system. However, over the past few decades, productivity has declined due to persistent climatic variability, severely affecting land use and groundwater reserves.

Regional studies have enhanced our understanding of these changes. For instance, Mahcer et al. (2024) analyzed NDVI variations (1983-2022) and found significant vegetation decline, while Bougara et al. (2021) identified trends toward wetter periods in the Tafna basin. Despite this progress, a critical link remains underexplored: the direct coupling between climate variability, land-use changes, and groundwater dynamics.

This research aims to fill this gap by analyzing the relationship between spatiotemporal climatic fluctuations, diachronic land-use changes—particularly in the main Wadi bed—and the response of the alluvial aquifer. The primary objective is to quantify how climate variability concurrently drives changes in both land cover and groundwater behavior, using standardized drought indicators to detect extreme events and shifts in rainfall regimes.

The article is organized as follows: the first section introduces the scientific context and objectives; the second describes the study area's characteristics; the third and fourth present the methodological framework and data processing; the fifth details the analytical methods; the sixth discusses the results and their implications; and the final section provides conclusions and recommendations for sustainable groundwater management.

To ensure clarity and consistency, key terms used throughout this study are defined as follows:

- Meteorological drought: A temporary but significant deficiency of precipitation compared to the long-term average, identified by negative Standard Precipitation Index (SPI) values. It is synonymous with rainfall deficit in this context.
- Rainfall deficit/excess: A quantitative measure (in percentage) of the departure of rainfall in a given period from a reference period, calculated using the method of Mahé and Olivry (1995). A negative value indicates a deficit, and a positive value indicates an excess.
- Climate aridity/dry period: A long-term structural condition of a region, characterized by low precipitation and high evaporative demand, leading to a permanent water deficit. In this study, it is quantified using the Climate Moisture Index (CMI).
- Groundwater recharge: The process by which water from precipitation infiltrates the soil and percolates downward to replenish an aquifer.

2. Study area

The region under study is located in the north-western part of Algeria, more precisely in the Wilaya of Mascara province, between 35º 15'-35º 50' N, and 0º-0º 40' E. This study focuses on the Wadi Fekan watershed, a sub-basin of the Macta, covering an area of 1194.38 km^2. The Wadi Fekan watershed corresponds to a strictly flat topographic zone, with border reliefs rising to an approximate altitude of 1178 m. It is bounded by the Beni-Chougrane Mountains to the north, the Saida Mountains to the south, Mount Oucilles (Djebel Âoussilâs) to the west, and the Tighenif Plateau to the east, as shown in Figure 1.

In addition, the Ghriss plain is an integral part of the basin under study. It should be noted that the irrigated lands of this plain constitute 56% of the total surface area of the Wilaya of Mascara.

The topographical features of the study area are defined by an elongated shape, with an average altitude of 589.60 m and a maximum height difference of 397 m, indicating a fairly strong relief. Furthermore, the drainage density of the watershed's hydrographic network is approximately 0.30 km^{-1}, indicating a relatively average network with a fairly long concentration time.

From a hydrogeological perspective, the region under investigation is characterized by a collapse basin with predominantly flat topography, surrounded by reliefs displaying a variety of geological features. The region under consideration is characterized by various layers, including quaternary alluvial deposits, lacustrine limestones, Pliocene sandstones, and upper Jurassic limestones.

3. The adopted approach

The primary objective of this study is to examine climate variability to highlight the extent of drought and/or wet conditions at both spatial and temporal scales. In addition, the study will analyse the consequences of this variability for water resources and land use in the Wadi Fekan watershed.

To characterize the spatiotemporal evolution of climatic conditions in the region under study, it was deemed necessary to utilize SPIs and CMIs. It is imperative to acknowledge the capacity of these indices to discern the period during which the disruption to the rainfall regime transpired. This interval then facilitates the calculation of the rainfall deficit, thereby enabling the monitoring of the temporal evolution of the climate. The results for the SPIs, CMIs, and rainfall deficit indices obtained for all stations were spatialised to highlight the spatial evolution of this phenomenon. Furthermore, the break detection tests were applied to the selected rainfall data series in order to validate the results of the statistical indices.

Furthermore, a study was conducted on the spatio-temporal evolution of water table fluctuations to determine the impact of spatio-temporal variability in climatic conditions on the water potential of the alluvial table. This study considered two main factors: groundwater overexploitation and the aquifer's hydrodynamic characteristics.

Finally, to confirm the results, a diachronic analysis of land use was conducted to examine possible changes driven by climate variability. This analysis enabled the study of the impact of the temporal climate evolution on land use.

4. Preparing and processing the data used

4.1 Climate data

All climate data were provided by the Algerian National Meteorological Office and the National Agency for Hydraulic Resources (ANRH), at a monthly time step.

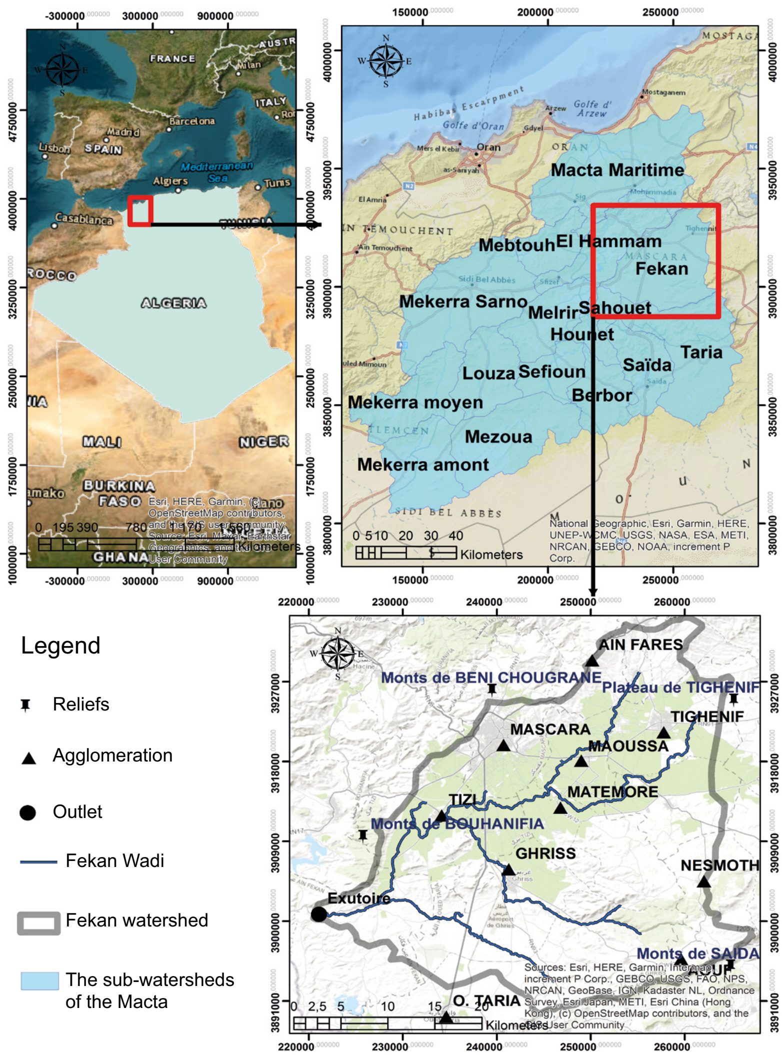

Fig. 1. Location of the study region.

4.1.1 Rainfall data

Rainfall information collected in the study area was obtained from 11 stations distributed appropriately within the Wadi Fekan watershed, as illustrated in Table I and Figure 2.

4.1.1.1 Choice of the study period

To ensure adequate rainfall representation in the region under study, it was deemed essential to adhere to the stipulated collection period, ensuring sufficient duration and minimal missing data. It is imperative to acknowledge the significance of this condition to comprehensively understand the climate's characteristics and accurately monitor its evolution. The inventory of missing data, by year and by rainfall station, is clearly depicted in Figure 3.

Most of the stations considered in this study experienced periods of shutdown during the Algerian War (1954-1962), while some of them were put back into service after 1962, which led to erroneous results, with a high number of missing data at the monthly and annual scales, as shown in Figure 3. Based on the above, it was decided to restrict the study period from September 1983 to August 2023, as this 40-year observation period presents a small number of gaps.

4.1.1.2 Filling in the missing data

The series of observations adopted in this work presents some missing data at the monthly and annual

Table I. Characteristics of the selected rainfall stations.

Code	Name	Coordinates (decimal degrees)		Operating period
		X	Y	
111429	Mascara	0.146428	35.39286	1983-2023
111405	Matemore	0.215025	35.329824	1944-2023
111401	Maoussa	0.248202	35.378314	1942-2023
111402	Froha	0.13004	35.303213	1944-2023
111417	Ain Fares	0.247782	35.481576	1969-2023
111413	Tizi	0.076127	35.320075	1969-2023
111201	Oued Taria	0.091058	35.115659	1908-2023
111414	Sidi Kada	0.344322	35.330201	1969-2023
111418	Nesmouth	0.381819	35.251571	1969-2023
111424	Ghriss	0.166501	35.246272	1973-2023
111217	Beniane	0.23145	35.101077	1969-2023

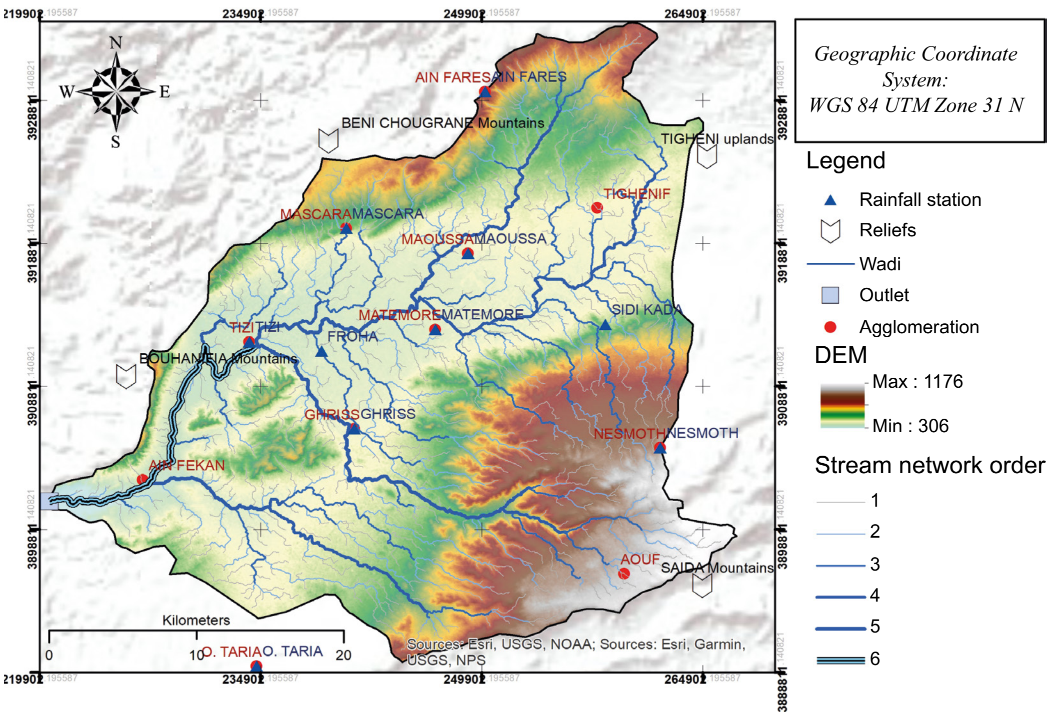

Fig. 2. Spatial distribution of rainfall stations.

scales (1983/84-2022/23). The missing data were completed using the simple linear regression method. It is useful to remember that this method neglects geographic reality and local rainfall nuances, which can lead to errors in judgment. For this, the climatic specificity of each station was taken into account to minimize these errors. Moreover, the stations that correlated best with each other (linear correlation) were grouped according to the weighting of the correlation coefficient for each month of the year (Laborde, 2007). Generally speaking, this method is applied by calculating a simple linear regression between the monthly series to be reconstructed and the complete monthly series of the surrounding stations. Let x and y be the two stations to be compared, and x(i) and y(i) their observations. It is considered that

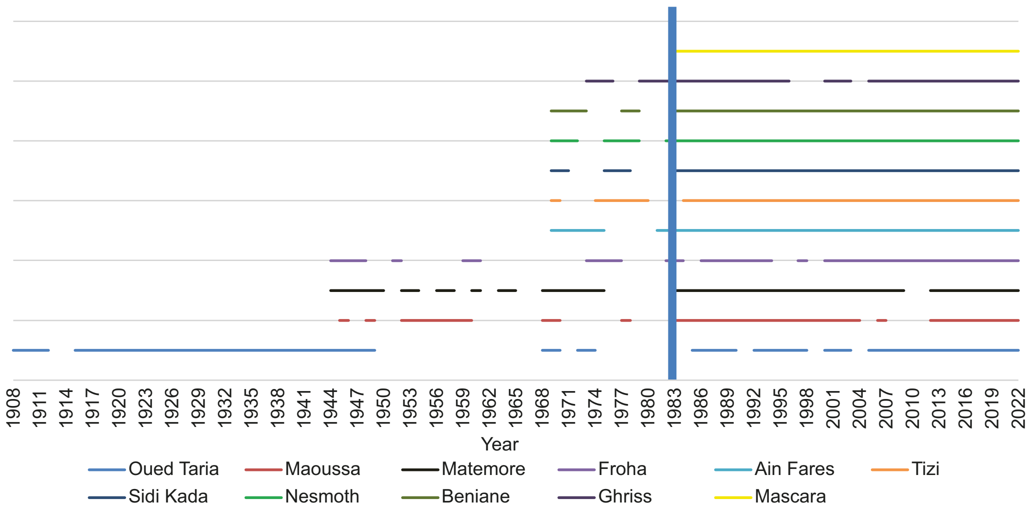

Fig. 3. Missing data by station and by year.

station x contains complete data of a given number of years, while station y contains complete data of a smaller number of years. Then, in order to fill in the missing year data from station y using the complete data from station x, it was deemed appropriate to apply the simple linear regression method.

The procedure consists of creating a $y(x)$ graph to get an idea of the bond's strength. If the cloud of points is elongated, with little dispersion around a central line, then it is possible to make a graphical adjustment of this dispersion. Therefore, the correlation coefficient can be calculated using the expression below:

$$r_{xy} = \frac{\sum \left[\left(x(i) - m_x \right) \left(y(i) - m_y \right) \right]}{\left(k - 1 \right) \left(\delta_x . \delta_y \right)} \tag{1}$$

where k is the number of values (or pairs) in the sample and the values of x and y are observed or measured simultaneously for each pair in the sample. Also, m_x is the average value of all x with $m_x = \frac{(\sum x(i))}{k}$, m_y is the average value of all y with $m_y = \frac{(\sum y(i))}{k}$, δ_x is the standard deviation of x with $\delta_x = \sqrt{\frac{\sum (x(i) - m_x)^2}{k-1}}$, and δ_y is the standard deviation of y with $\delta_y = \sqrt{\frac{\sum (x(i) - m_x)^2}{k-1}}$

For a significant correlation, the equation of the regression line can then be written as:

$$y(x) = m_y + r_{xy} . \frac{\delta_y}{\delta_x} . \left(x - m_x \right)$$

which is in the form:

$$y(x) = a\,x + b \tag{2}$$

with $a = r_{xy} . \frac{\delta_y}{\delta_x}$ and $b = m_y - m_x . r_{xy} \frac{\delta_y}{\delta_x}$

4.1.2 Potential evapotranspiration

The potential evapotranspiration can be calculated using the formula developed by Turc (1954). It is given below as:

$$ETP = \left(Ig + 50 \right) k \frac{t}{t + 15} \quad \text{Ou } k = 0.013n \tag{3}$$

where ETP is the monthly potential evapotranspiration (mm), t is the monthly average air temperature (ºC), and Ig is the monthly average global radiation at the ground surface (in calories cm^{-2} day^{-1}).

It should be noted that $Ig = IgA \left(0.18 + 0.62 \frac{h}{H} \right)$, where IgA is the theoretical global radiation (calories cm^{-2} day^{-1}) and H is the theoretical duration of the days of the month, k is a coefficient equal to 0.37 for the month of February and 0.40 for the other months, and n is the number of days in the month.

4.2 Geospatial data

4.2.1 Piezometric data

The alluvial aquifer of the Ghriss plain has been the subject of several piezometric measurement campaigns by the ANRH since 1970. In the present study, the focus was exclusively on the piezometric maps established during the high-water periods, i.e., the months of March and April, for the years 1977, 1987, 1998, 2007, and 2018, as illustrated in Figure 4.

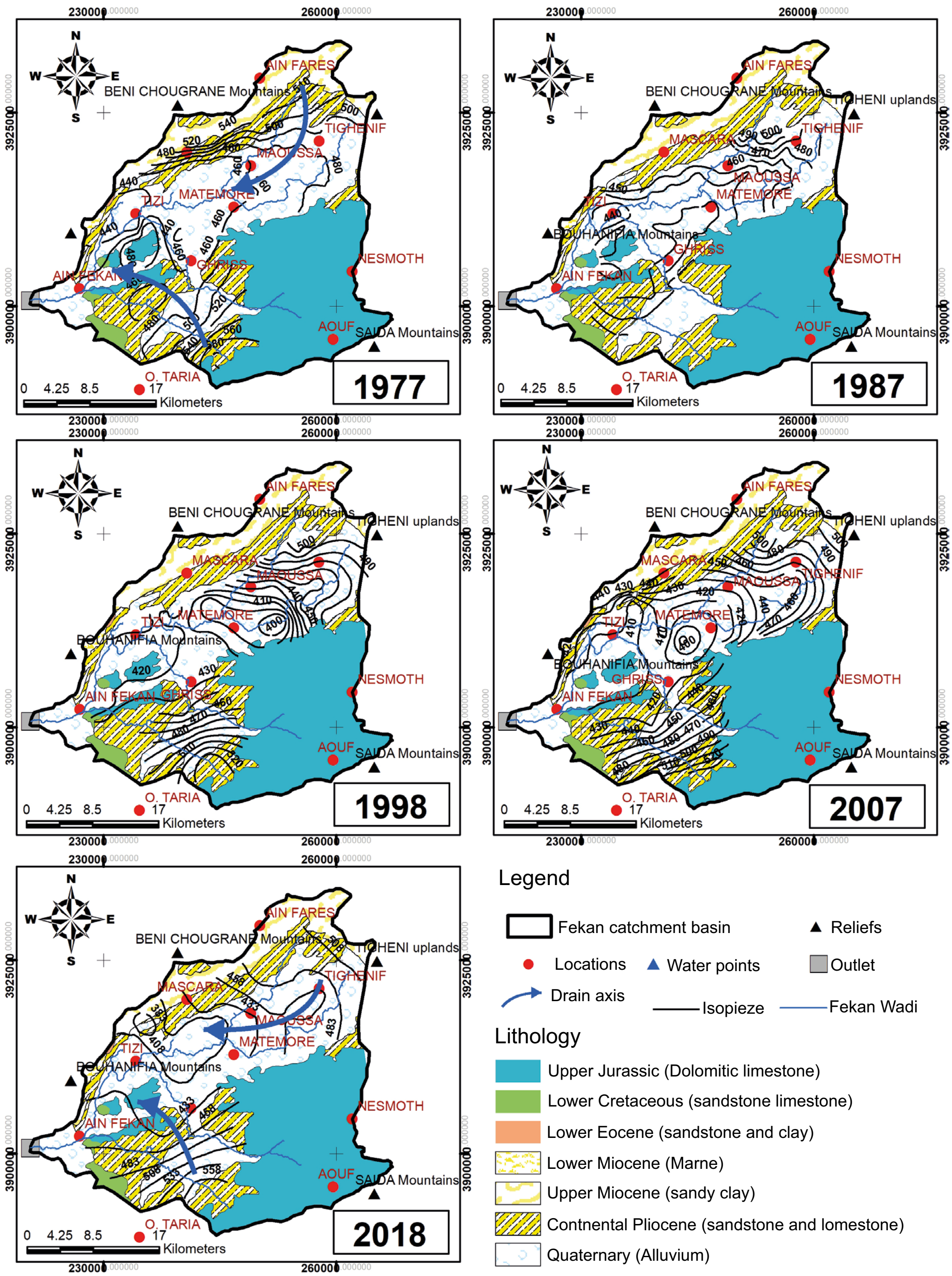

Fig. 4. Spatiotemporal evolution of the piezometer of Ghriss plain at high waters, in the Wadi Fekan basin.

The analysis of the piezometric maps indicates that the convergence of underground and surface flows towards the Ain Fekan outlet is perfect, thereby confirming the permanent relationship between the aquifer and Wadi Fekan. Furthermore, the hydraulic gradient is weak for the alluvial part of the plain, while it is strong in the relief zones, at the edge of the alluvial plain.

The general appearance of the piezometric maps retained, as well as the arrangement of the isopiez curves, reveals an open limit to the north of the alluvial layer, which explains the supply from the continental Pliocene sandstone and limestone. However, it has been revealed that this regime became increasingly rare from 1998 to the end of the observation period. It is also noteworthy that the isopiez curves are arranged perpendicular to the continental Pliocene formations.

4.2.2 Physical characteristics of the alluvial layer

The transmissivity of the aquifer is widely accepted as a reliable metric for its overall productivity. In this regard, the water table is regarded as more transmissive in cases of low drawdown, i.e., the difference between the static and dynamic levels in the aquifer. Conversely, during substantial drawdowns, the water table is reputed to exhibit reduced transmissivity. These observations were then utilized to establish the spatial evolution based on hydrodynamic data of 51 water points that are well distributed across the study area (see Fig. 5 and Table SI in the supplementary material). This objective was accomplished by adopting the most recommended geostatistical method in hydrogeology, namely ordinary kriging (Gratton, 2002). According to Nur'eni et al. (2020) and the researchers from the GeoRGB Community (2023), this method is considered the most accurate for justifying geological and hydrogeological studies.

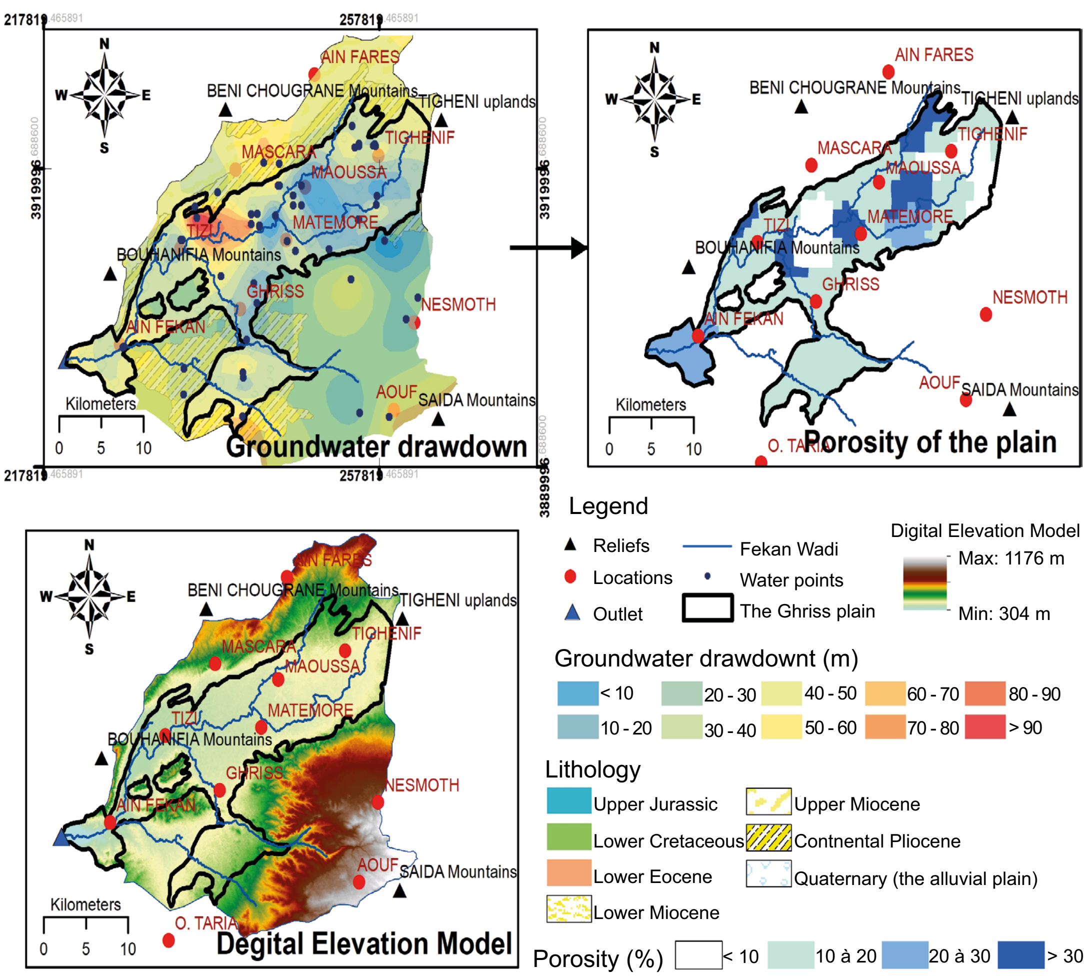

Fig. 5. Physical characteristics of the alluvial water table.

The detailed parameters of the variogram model used, namely nugget, partial sill, and range, are presented in Table SIV.

This method has several advantages, including:

- Accuracy.
- Flexibility.
- Interpretability.
- Efficiency.
- And the possibility of updating the model.

However, it also has certain limitations, such as:

- Its dependence on data quality.
- Its sensitivity to the choice of parameters.
- Its difficulty in dealing with non-stationary data,
- Incomplete spatial uncertainty.

Furthermore, an analysis of the spatial distribution of the drawdown demonstrates a high degree of congruence with the porosity map established by Baba-Hamed et al. (2015) during the calibration of their transient hydrodynamic model, as illustrated in Figure 5. Indeed, the aquifer productivity is mainly concentrated in the environs of Matemore and Maoussa, where porosity is significant (> 30%). However, low porosity values are encountered near the village of Tizi, thus implying a low transmissivity that is represented in the form of a very significant drawdown.

It can therefore be asserted that the filling of Ghriss plain is characterized by alluvial heterogeneity, which then conditions the spatial variability of effective porosity and, consequently, that of hydrodynamic parameters such as transmissivity and storage coefficient.

The following essay will provide a comprehensive overview of the relevant literature on the subject.

4.2.3 Satellite data

The land use maps were produced using ENVI 5 software, based on images from the Landsat 7 and 8 satellite sensors, acquired in 1987 and 2018 during high-water periods (Table II). The satellite images were then processed and corrected after being downloaded from the free website http://earthexplorer.usgs.gov. Table II provides a synopsis of the characteristics of the two images employed in this study.

5. Method used

The analysis of the temporal evolution of average annual rainfall, recorded at all selected stations during the observation period from 1983/84 to 2022/23, reveals a clear variability that can be thoroughly studied through rainfall sequences. This objective can be accomplished by dividing the observation period into multiple decades: 1983/84 to 1992/93, 1993/94 to 2002/03, 2003/04 to 2012/13, and 2013/14 to 2022/23. The average rainfall for each period was found to be 286.9, 309, 419.6, and 372 mm, respectively, as shown in Figure 6.

Table II. Characterization of satellite images.

Path	Row	Date	Sensor	Mode	Spectral bands		
					Band	Spectral band (µm)	Spatial resolution
197	36	Januaery 2, 1987	Landsat 7 (ETM^+)	Multispectral	4 (Infrared)	0.772-0.898	30 m
					3 (Red)	0.631-0.692	30 m
					2 (Green)	0.519-0.601	30 m
					1 (Blue)	0.441-0.514	30 m
197	36	January 21, 2018	Landsat 8 (OLI)		5 (Infrared)	0.851-0.879	30 m
					4 (Red)	0.636-0.673	30 m
					3 (Green)	0.533-0.590	30 m
					2 (Blue)	0.452-0.512	30 m

ETM+: Enhanced Thematic Mapper; OLI: Operational Land Imager.

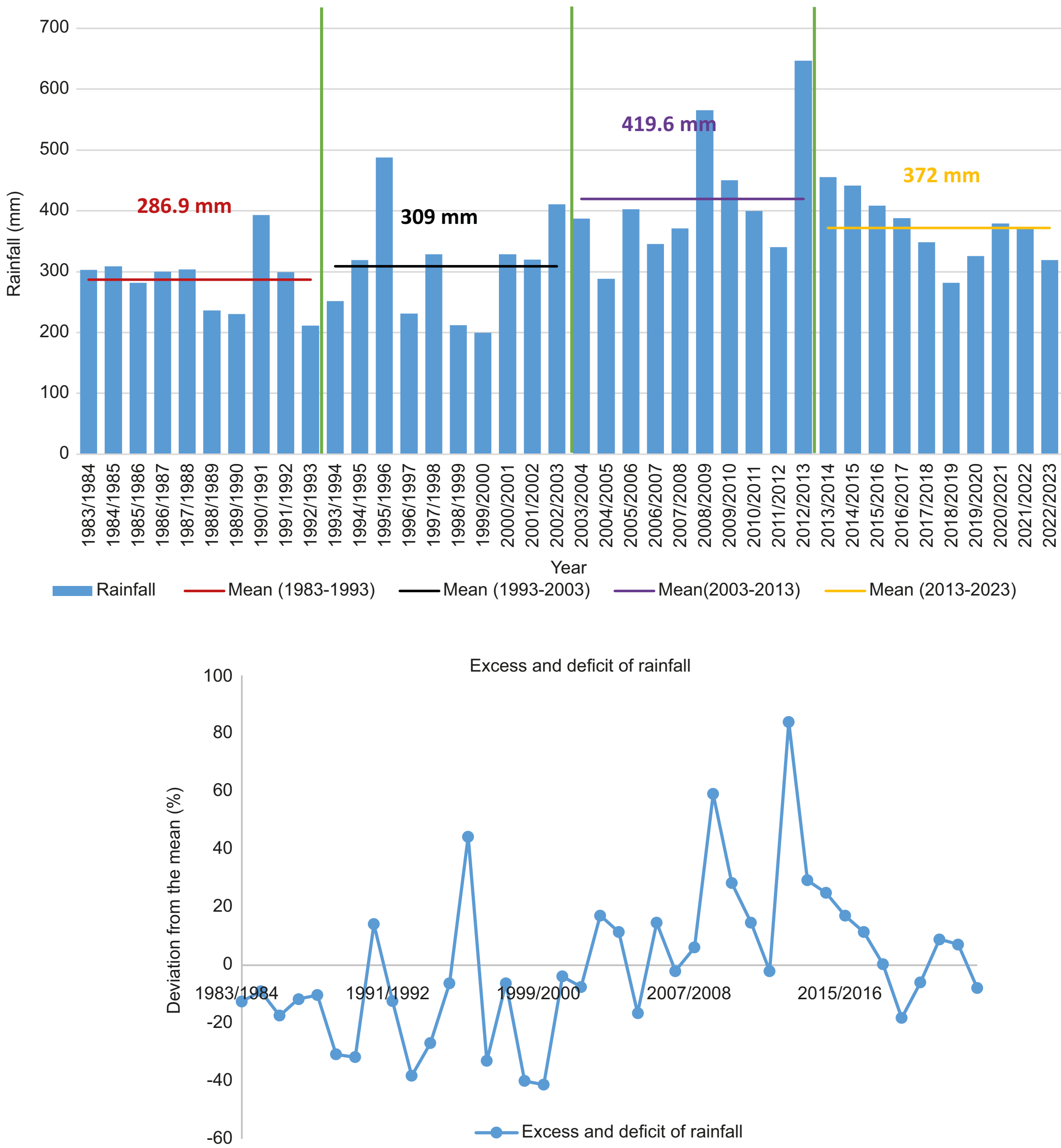

Fig. 6. Temporal evolution of average annual rainfall recorded at the 11 selected stations (1983/84-2022/23).

5.1 Standardized precipitation index

The SPI, developed by McKee et al. (1993), is a widely used indicator for quantifying meteorological drought. It is a probability-based index that relies exclusively on precipitation data. SPI values are standardized such that a value of 0 corresponds to median precipitation, relative to a long-term reference climatology typically calculated over a 30- to 40-year period.

The index has been applied in numerous studies worldwide (e.g., Wu et al., 2001; Giddings et al., 2005; Sonmez et al., 2005; Bodian, 2014), owing to its simplicity and adaptability across climatic zones.

The SPI can be computed using the following formula (Lamb, 1982):

$$SPI = \frac{(P_i - P_m)}{\sigma_i} \tag{4}$$

where P_i is the precipitation in year i, P_m is the mean annual precipitation over the reference period, and σ_i is the standard deviation of annual precipitation. To determine the severity of drought (or wetness) for each year in the time series, standard SPI classification thresholds are used, as summarized in Table III (Wu et al., 2001).

Table III. Classification of drought in relation to the SPI values.

SPI class	Climate phenomenon
SPI > 2	Extreme humidity
1 < SPI < 2	Severe humidity
0 < SPI < 1	Moderate humidity
-1 < SPI < 0	Moderate drought
-2 < SPI < -1	Severe drought
SPI < -2	Extreme drought

SPI: standardized precipitation index.

This classification has also been adopted in several research works (Ardoin et al., 2003; Dao et al., 2010), as it allows determining the percentage of years per SPI class, thereby highlighting the extent of drought or wetness events.

5.2 Climate moisture indices

It is essential to study the evolution of the CMI to better understand potential changes in the regional climate regime. The CMI is a widely used indicator that combines annual precipitation (P) and potential evapotranspiration (ETP) to provide insight into the climatic water balance. It yields values ranging between –1 and +1, allowing for easy interpretation of climate conditions.

The index is calculated using the following conditional formula (Willmott and Feddema, 1992):

$$CMI = \begin{cases} \frac{P}{ETP} - 1 & \text{if } P < ETP \\ 1 - \frac{ETP}{P} & \text{if } P > ETP \end{cases} \quad (5)$$

An equivalent and more compact form of the CMI is:

$$CMI = \frac{P - ETP}{P + ETP} \quad (6)$$

where P is the annual precipitation, and ETP is the annual potential evapotranspiration.

As with the SPI, CMI values are grouped into distinct classes to identify prevailing climatic conditions in a given area (Willmott and Feddema, 1992; Vörösmarty et al., 2005). The classes are defined as follows:

$$\begin{cases} CMI > 0 & \text{Humid} \\ -0.6 \;\; CMI \;\; 0 & \text{Semi-arid} \\ CMI \;\; -0.6 & \text{Arid} \end{cases} \quad (7)$$

This classification allows the identification of dominant climate types within the basin over specific time periods, which is crucial for assessing the region's vulnerability to climate variability and drought.

5.3 Rainfall deficit or excess index

The extent of drought or humidity is determined based on the SPI and CMI, and complemented by the calculation of rainfall deficit or excess. Negative values indicate a deficit, while positive values correspond to an excess. The method is based on calculating the percentage of variation in the mean around the break date. The formula for calculating the rainfall deficit or excess index was established by Mahé et al. (1995):

$$D = \left(\left(\frac{\bar{X}_j}{\bar{X}_i} \right) - 1 \right) 100 \quad (8)$$

where D is the rainfall deficit or excess, $\bar{X}_i$ is the average of the period before the break, and $\bar{X}_j$ the average of the period after the break.

The calculated indices were then geostatistically spatialised using the Spline method, which proved effective in identifying the regions most vulnerable to climate variability.

5.4 Break detection tests

Several researchers, including Bois (1971), Brunet-Morel (1977), Buishand (1982), and Lubès et al. (1994), define a break as a change in the statistical distribution of a time series—specifically, a significant shift in the mean or variance. In many cases, both types of changes may occur simultaneously at an unknown point in the series. According to Beaulieu et al. (2008), these changes often reflect underlying climate variability or transition processes and are typically investigated through tests of stationarity and randomness.

In this study, the detection of shifts in the mean precipitation values was conducted using a combination of parametric and non-parametric methods: (1) the Lee and Heghinian (1977) Bayesian test, which is suitable for normally distributed series; (2) the Pettitt (1979) test, a robust non-parametric test based on the Mann-Whitney U statistic (Dagnelie, 1970); and (3) the Hubert segmentation test (Hubert et al., 1989; Hubert, 2000; Beaulieu, 2009), which allows to detect multiple change points in the mean. These tests were specifically chosen for their methodological complementarity and robustness (Lubes et al., 1998; Niang et al., 2008). The Pettitt test is effective for detecting single change points in non-normal or non-parametric time series, making it suitable for hydrometeorological data. The Lee and Heghinian test, with its Bayesian framework, provides a probabilistic assessment of change for normally distributed series. Finally, the Hubert segmentation method is particularly powerful for identifying multiple shifts, which is critical for long climate series exhibiting several phases of variability.

Their performance and reliability have been confirmed in several hydroclimatic studies across Africa (e.g., Paturel et al., 1998; Kingumbi et al., 2001; Goula and Adamopoulos, 2005; Djellouli, 2017; Gherissi, 2018), where they demonstrated strong diagnostic capability in identifying climate shifts in rainfall series.

The Khronostat software, developed at the Montpellier Research and Development Institute (Boyer, 2002), was used to implement these statistical procedures. It facilitated the visualization, calculation, and storage of results in digital format, streamlining the analytical workflow and ensuring reproducibility.

5.5 The spatiotemporal fluctuation of the water table

Climatic variability can lead to more severe consequences due to its effects on the groundwater potential of the alluvial aquifer in the plain of Ghriss. The procedure adopted here consists of determining the water table fluctuation over the same sub-periods used for the statistical indices. For this, the piezometric maps established in the same season were used to determine the spatial fluctuation of the water table between 1987 and 1977, 1998 and 1987, 2007 and 1998, 2018 and 2007, and finally between 2018 and 1987. The approach used consists of superimposing the piezometric maps of the years 1987, 1998, 2007, 2018, and 2018 with those of the years 1977, 1987, 1998, 2007, and 1987, respectively, under a geographic information system (GIS), in order to determine the points of intersection that represent the drawdowns. It should be noted that if the values obtained are positive, we have a supply from the water table, but if they are negative, a drawdown is observed. The spatialization of the results obtained using the ordinary kriging method gives, for each period, a map representing the spatio-temporal evolution of the water table fluctuation, as illustrated in Figure 14.

5.6 Land use

Land cover mapping was carried out using a supervised classification based on the maximum likelihood algorithm applied to two satellite images: one acquired in 1987 by the Landsat 5 (TM) sensor and the other in 2018 by the Landsat 8 (OLI) sensor. All available spectral bands were utilized for both images (Richards and Jia, 2006).

To ensure balanced spatial representation, dozens of training samples were evenly distributed across the entire study area.

Class assignment was based on expert photo-interpretation: for the 1987 image, this process relied on local field knowledge and topographic maps from the same period. For the 2018 image, interpretation was supported by Google Earth imagery, whose spatial accuracy has been demonstrated in the literature (Potere, 2008).

The methodological approach followed three main steps:

1. Initial visual interpretation of landscape features based on their spectral and contextual characteristics.
2. Selection of representative training areas for each target class.
3. Evaluation of classification accuracy using a confusion matrix, along with the calculation of related performance metrics.

The results showed highly reliable classification, with an overall accuracy of approximately 90.0% in 1987 and 92.0% in 2018. The

Table IV. Characteristics of the main land cover classes according to the RGB color composition that was produced from Landsat channels.

Water	Agriculture	Bare soil	Built	Dense forest	Light forest	Course
Dark to light blue (clarity increasing with turbidity)	Chlorophylls: magenta Chlorophylls: brown-green	More or less light blue or cyan	Very light blue to white	Dark brown	More or less light brown	Very light magenta

corresponding Kappa coefficients were 0.8025 and 0.839, respectively, indicating strong agreement between the classified data and the ground truth. The Kappa coefficient (κ\kappaκ) quantifies the level of agreement between the classification and the reference data, while accounting for chance agreement (Cohen, 1960). It is defined by the following equation:

$$\kappa = \frac{P_o - P_e}{1 - P_e} \quad (9)$$

where P_o is the observed overall accuracy (the ratio of correctly classified pixels to the total number of pixels), and P_e is the expected accuracy by chance, calculated from the marginal totals of the confusion matrix.

In total, seven land cover classes were identified, enabling clear distinctions between water bodies, vegetation types, and bare soil surfaces (see Table IV). The confusion matrices for 1987 and 2018, along with full class-wise accuracies and parameters, are provided in Tables SV and SVI in the supplementary material.

6. Results and discussion

6.1 Standardized precipitation index

The SPIs from the various stations within the study region were analyzed. The region under discussion may be considered to represent any geographical area within western Algeria. Indeed, the findings of this study indicate a consistent temporal evolution, with a break detected towards positive values, which began to occur with greater frequency during the period between 2000 and 2006 (see Fig. S1 for further details). These observations provide substantial justification for adopting the four preceding decades (1983-2023).

Furthermore, analysis of the SPI results obtained for all the stations selected reveals the dry climatic character of the study region during the decades 1983-1993 and 1993-2003, in comparison with the last two decades of the observation series (see Table V and Fig.7). Indeed, this moderate, severe, or extreme drought can reach worrying values. The drought rate could reach 75.5% during the decade 1993-2003, during which severe drought began to increase (25.5%). In parallel, conditions classified as moderate, heavy, and extreme wetness are collectively minimal and are represented as infrequent occurrences. The moderate humidity conditions in this region range from 22.7 to 16.4%, the high humidity conditions from 2.7 to 3.6%, and the extreme humidity conditions from 0.1 to 4.5%.

Conversely, during the final two decades of the observation series (2003-2013 and 2013-2023), the study region experienced significant wet conditions, particularly during the 2003-2013 decade, with extreme, high, and moderate humidity levels reaching 15.5, 10.9, and 40%, respectively. However, the final decade of the series (2013-2023) was marked by a mix of moderate humidity and drought, with a notable prevalence of wet conditions.

It was also noted that during the wet periods (2003-2013 and 2013-2023), the study region did not experience strong or extreme drought conditions, since only moderate drought was recorded, accounting for only 32.7 to 34.5% of the cases.

It is evident from these results that the study region experienced an exceptional rainfall regime during the decade 2003-2013, characterized by a high humidity rate that reached its peak during that period. This regime thus represents approximately one quarter of all the climatic conditions observed during this decade. Additionally, it was observed that the combined effect of high and extreme humidity does not surpass 8% across the remaining decades of the observation series (i.e., the dry decades).

Table V. Percentage of years for each SPI class, for all the stations selected, during the period between 1983/84 and 2022/23.

SPI class	Drought degree	Dry period				Humid period				1983-2023	
		1983-1993		1993-2003		2003-2013		2013-2023			
SPI > 2	Extreme moisture	00.1		04.5		15.5		00.9		05.2	
1 < SPI < 2	High moisture	02.7	**25.5**	03.6	**24.5**	10.9	**66.4**	08.2	**65.5**	06.4	**45.5**
0 < SPI < 1	Moderate moisture	22.7		16.4		40.0		56.4		33.9	
–1 < SPI < 0	Moderate drought	43.6		49.1		32.7		34.5		40.0	
–2 < SPI < –1	High drought	30.9	**74.5**	25.5	**75.5**	00.9	**33.6**	00.0	**34.5**	14.3	**54.5**
SPI < –2	Extreme drought	00.0		00.9		00.0		00.0		00.2	
Total		100%		100%		100%		100%		100%	

SPI: Standard Precipitation Index. Figures in bold represent the total percentage of humidity/dryness.

The spatial distribution of the SPIs across the selected periods suggests a marked drought between 1983 and 2003, followed by a comparatively wet period between 2003 and 2023. During this period, the drought is more geographically constrained, as illustrated in Figure 8. Consequently, the spatial evolution of climatic conditions over the entire observation period (from 1983 to 2023) highlights the presence of some humidity along the basin periphery, thereby explaining the Foehn effect caused by the watershed crest lines (see Fig. 8).

The SPI analysis clearly demonstrates the usefulness of this method in identifying temporal and spatial drought patterns. It highlights the predominance of drought conditions between 1983 and 2003, followed by a wetter regime after 2003. These results directly validate the application of SPI in the Oued Fekan watershed, as it allows distinguishing long-term climatic phases and linking them with observed groundwater fluctuations.

6.2 Climatic moisture index

The temporal evolution of the climatic CMIs for the selected stations shows that, in general, the region under study did not experience any humid conditions (i.e., CMI > 0) during the observation period considered (i.e., absence of positive CMI values, as indicated in Fig. S2 and Table V). However, the arid climatic regime strongly characterizes the initial two decades, with 88.2 and 78.2% of the cases, respectively, for the decades 1983-1993 and 1993-2003. Conversely, over the past two decades, the rate of aridity has declined concurrently with a substantial expansion of semi-arid climatic conditions. The period from 2003 to 2013 saw the highest number of aridity cases, accounting for 43.6% of the total cases occurring during this decade. The results of this study are presented in Table VI.

The region under scrutiny thus experienced climatic variability. The area transitioned from a strictly arid regime during 1983-2003 (88.2 to 78.2%) to a semi-arid regime (2003-2023), with a subsequent trend towards aridity. Moreover, the proportion of semi-arid conditions was estimated at 43.6% of cases during the period 2003-2013, and 36.4% during the period 2013-2023, as shown in Figure 9.

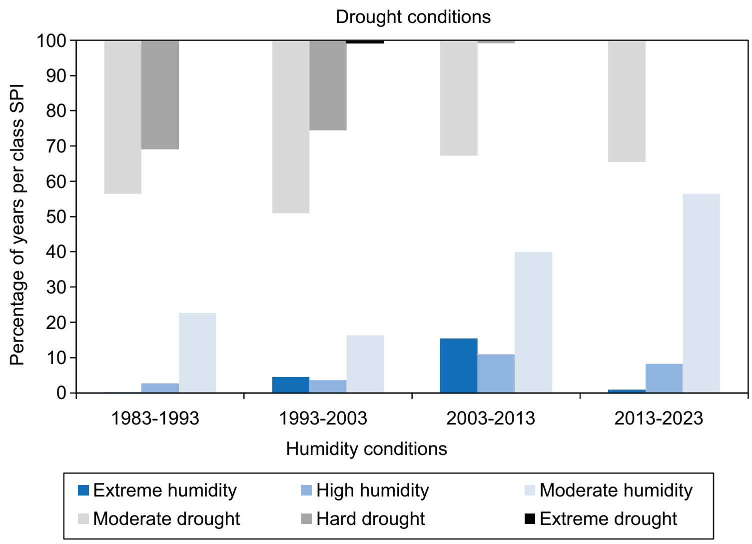

(a)

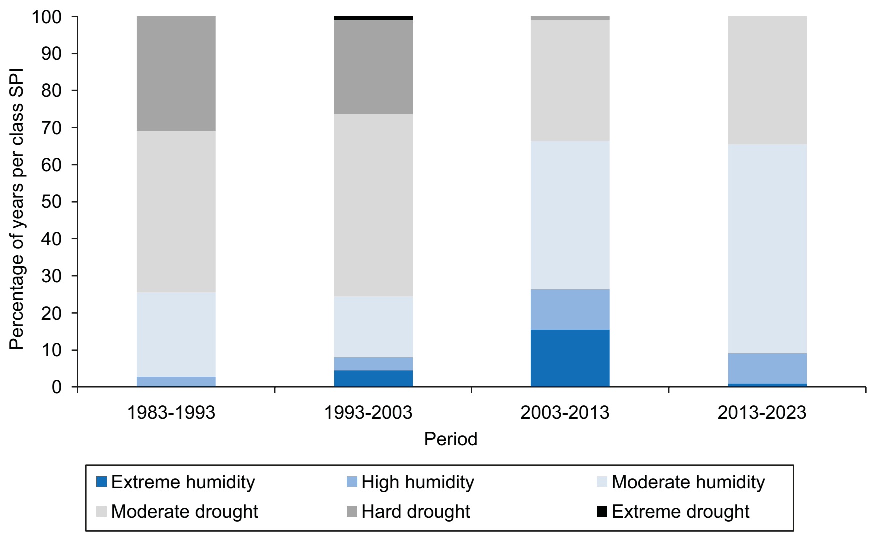

(b)

Fig. 7. (a) Evolution of wet and dry climatic conditions, and (b) rate of each phenomenon, through the different periods of the observation series.

The spatial distribution of CMI values indicates that the climate becomes increasingly arid towards the centre of the basin, where the climatic conditions are more severe (high temperatures). However, the basin's end is characterized by relatively moderate aridity, a consequence of the mountains of Saida, Béni Chougrane, and Bouhanifia. As illustrated in Figure 10, the CMI undergoes a spatiotemporal evolution. It is evident that the data sets under consideration both demonstrate and elucidate the humidity levels experienced during the period 2003-2013.

The CMI provides a complementary perspective by integrating both precipitation and evapotranspiration. It confirms the predominance of arid conditions before 2003 and a relative shift towards semi-aridity afterwards. This approach is essential for understanding recharge potential, as it directly links climate balance to aquifer replenishment.

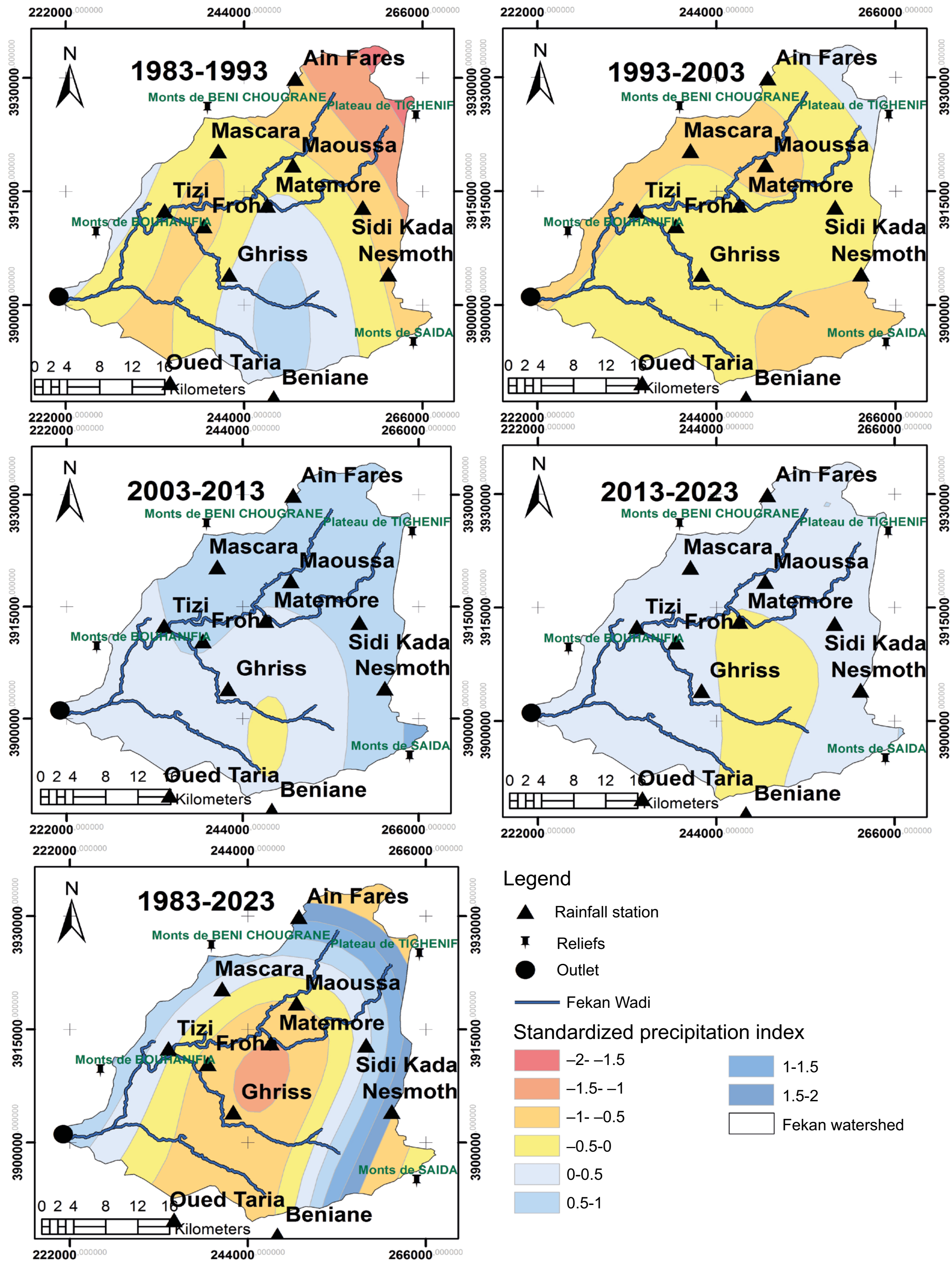

Fig. 8. Spatiotemporal evolution of Standard Precipitation Indices (SPIs) during the period from 1983/84 to 2022/23.

Table VI. Percentage of years for each CMI class, for all the selected stations during the period between 1983/84 and 2022/23.

CMI class	Climate type	Dry period		Humid period		1983-2022
		1983-1993	1993-2003	2003-2013	2013-2023	
CMI > 0	Humid	00.00	00.00	01.90	00.00	00.50
–0.6 < CMI < 0	Semi-arid	11.80	21.80	43.60	36.40	28.40
CMI < –0.6	Arid	88.20	78.20	54.50	63.60	71.10
Total		100.00	100.00	100.00	100.00	100.00

CMI: Climate Moisture Index.

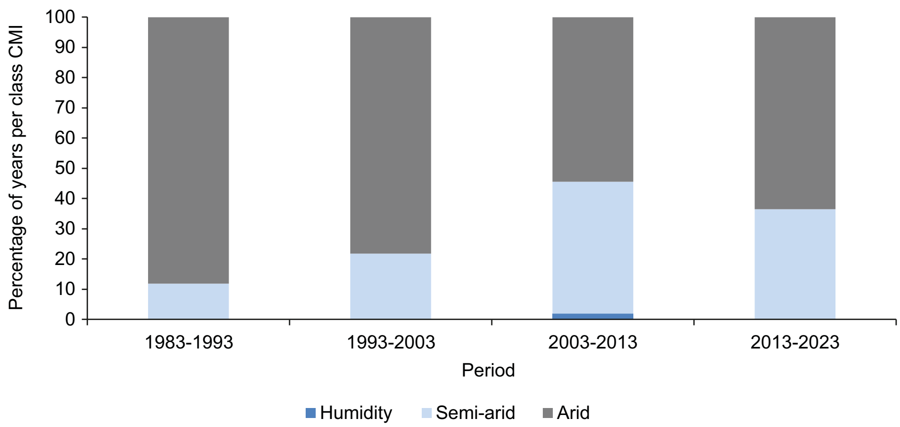

Fig. 9. Temporal evolution of arid and semi-arid climatic conditions, and rates of each phenomenon, during the different periods of the observation series.

6.3 Rainfall deficit or excess index

The average excess rainfall during the period 1983-2003 for all selected stations reached its maximum during 2003-2013, with more than 39.5%. This transition towards a drier environment appears less evident during the period 2013-2023, characterized by a minimal increase in rainfall, with a maximum excess of 24% (see Table VII).

The spatial distribution of the excess rainfall index, compared with the dry period (1983-2003), generally follows the same distribution as that of the CMIs for the two periods under consideration, as presented in Figure 11. Indeed, the deficit reaches –20% in the centre of the basin (i.e., near Ghriss), with a remarkable spatial evolution during the decade 2013-2023 in the regions of Ghriss, Froha, and Matemore. However, the remainder of the basin experienced an evolving excess of rainfall as it moved upstream (heights), reaching exceptional values during the decade 2003-2013. It has been demonstrated that these values have the capacity to exceed 50% (in regions such as Ain Fares, Sidi Kada, and Nesmoth), or even 85% at the Beniane station. Conventionally, during the period 2013-2023, the excess rainfall did not exceed 43%, as demonstrated in Table VII and Figure 11. The spatial evolution of the excess rainfall generally shows a progressive decrease from the northeast to the southwest of the basin. A particularity is observed in the centre, where rainfall deficit is evident. This deficit is attributed to the Foehn effect, which is caused by the mountains of Saida and Beni-Chougrane, and by the Tighenif plateau.

The rainfall deficit/excess index quantifies alternating surpluses and deficits. It identifies the exceptional recharge potential between 2003-2013 and its subsequent decline, providing a clear measure of climatic stress on aquifer renewal. This method

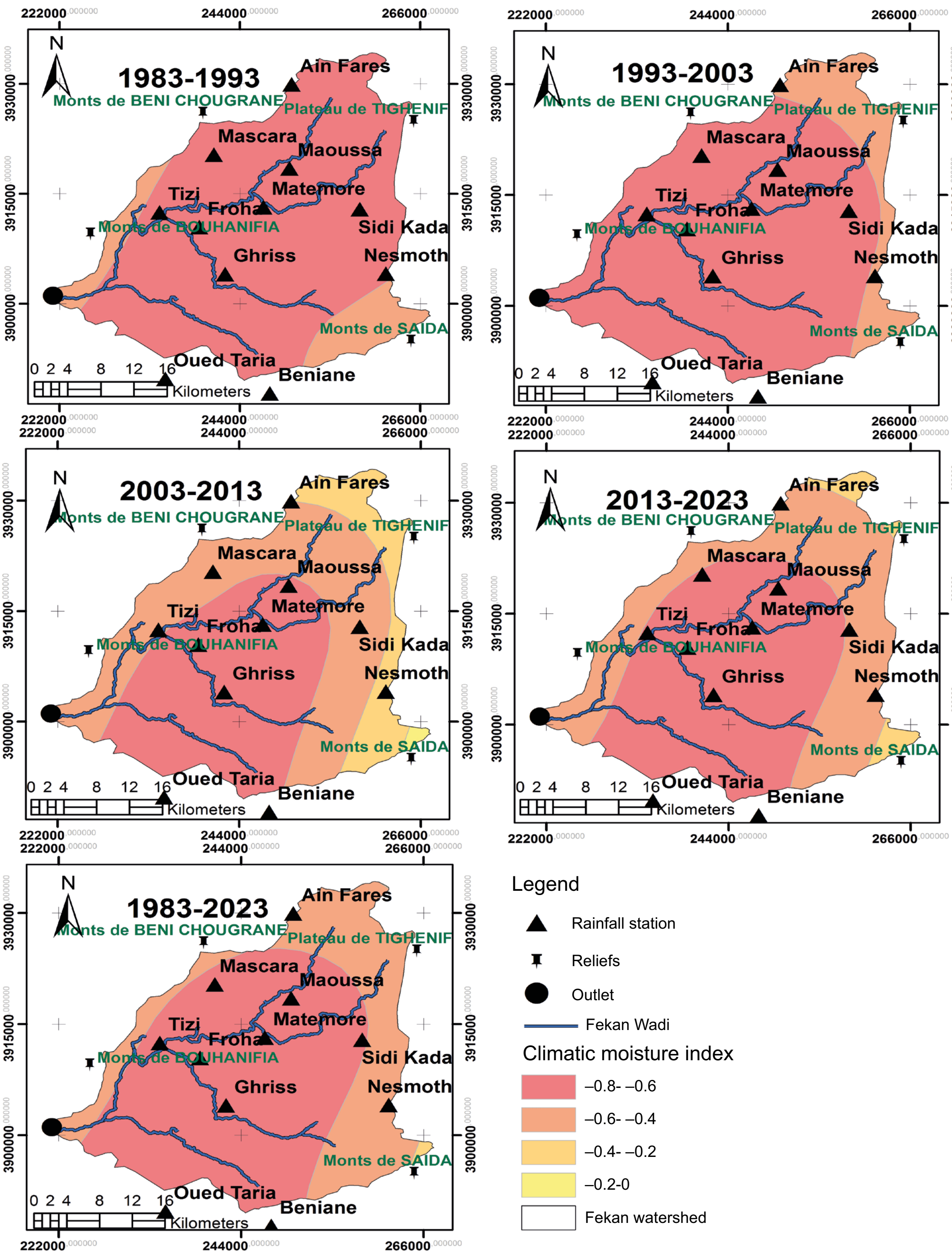

Fig. 10. Spatiotemporal evolution of aridity based on Climate Moisture Indices (CMIs) during the period extending from 1983/84 to 2022/23.

Table VII. Percentage of rainfall surpluses during the decades 2003-2013 and 2013-2023, as compared to the decade 1983-2003.

Station	Rainfall (1983-2003)	Period 2003-2013		Period 2013-2023	
		Rain (mm)	Excess (%)	Rain (mm)	Excess (%)
Mascara	305.3	447.0	+46.4	388.2	+27.2
Matemore	265.6	300.2	+13.0	272.5	+2.6
Maoussa	273.3	369.9	+35.3	332.4	+21.6
Froha	268.0	340.5	+27.0	318.7	+18.9
Ain Fares	369.5	574.9	+55.6	527.0	+42.6
Tizi	323.5	393.6	+21.6	381.2	+17.8
Oued Taria	256.4	314.6	+22.7	301.6	+17.6
Sidi Kada	310.7	472.2	+52.0	399.9	+28.7
Nesmoth	383.0	638.0	+66.6	530.8	+38.6
Ghriss	267.4	293.2	+9.7	288.3	+7.8
Beniane	254.5	471.8	+85.4	351.0	+38.0
Average	297.9 mm	419.6 mm	**+39.58%**	372 mm	**+23.77%**

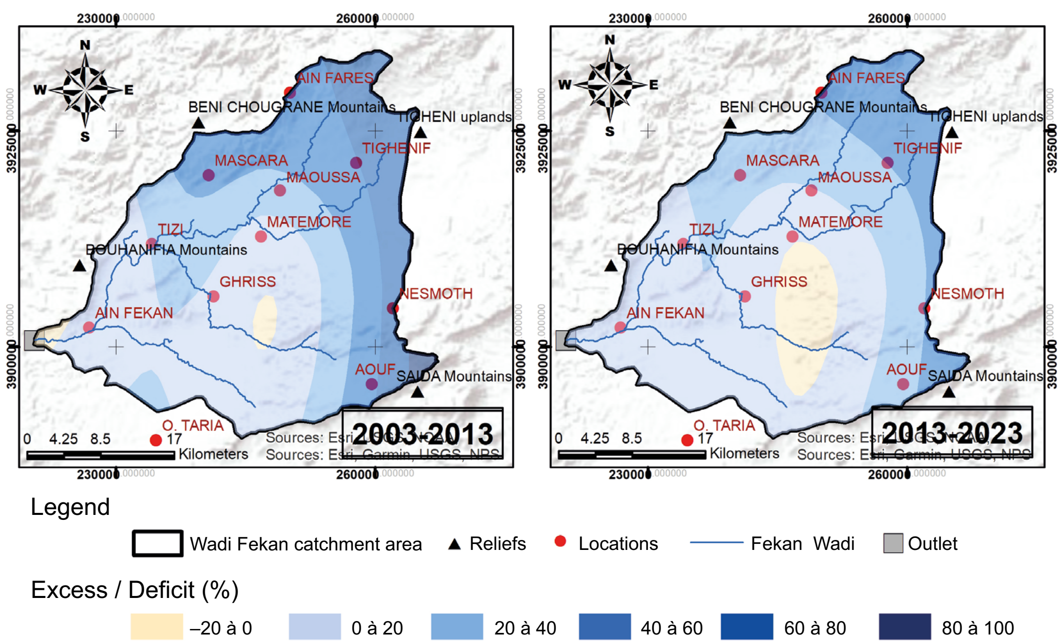

Fig. 11. Spatiotemporal evolution of rainfall deficits and excesses (%), during the periods 2003-2013 and 2013-2023, as compared to that of 1983-2003.

therefore directly connects climatic variability with the availability of effective recharge.

6.4 Break detection tests

The substantial number of wet years, as determined by the aforementioned indices, was confirmed through break-detection tests. As demonstrated in Figure 12, the tests were conducted, and the results obtained at the various stations are presented therein. The findings of this study indicate a significant deviation from the expected trend during the period spanning from 1999 to 2006. Furthermore, the findings of the present study corroborate the hypothesis that a wetter regime of the annual rainfall module has become a reality,

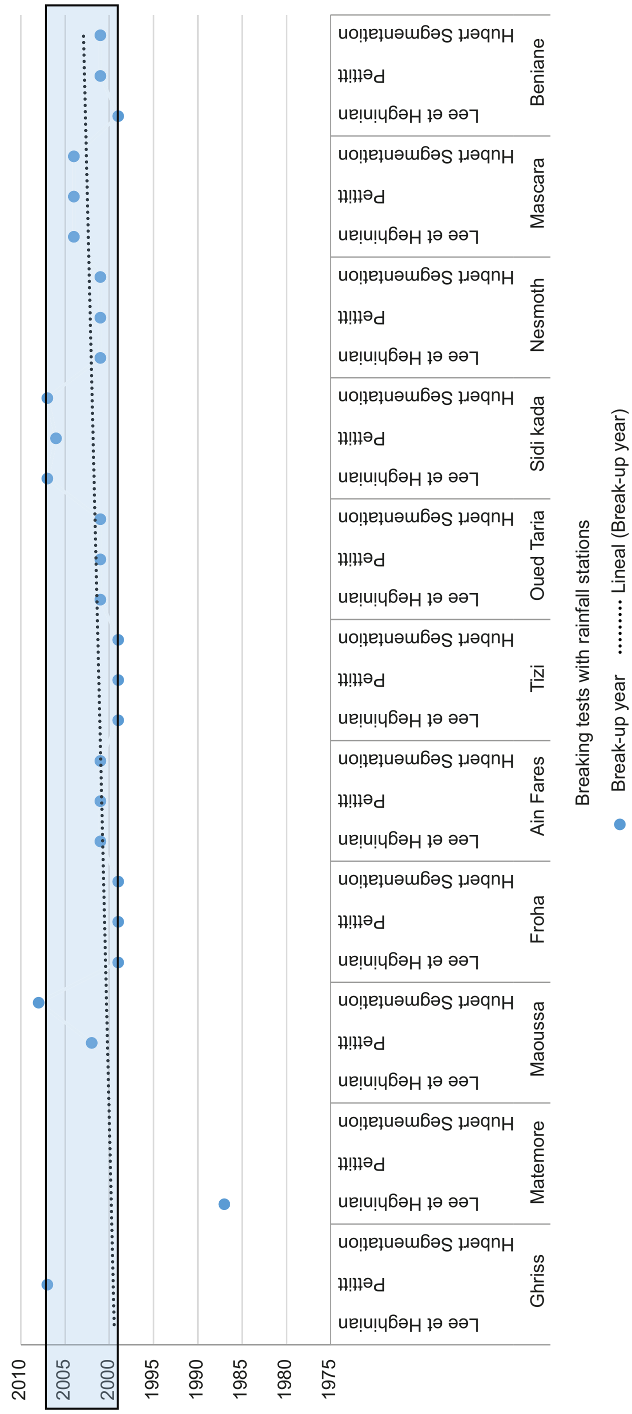

Fig. 12. Years of ruptures from the different tests, at the different stations selected.

with an average excess of 36.41% (see Table SII). As demonstrated, a deficit sequence was identified during the period of observation, characterised by significant precipitation. This sequence was identified using the Hubert segmentation test and was present between 2013 and 2014. The analysis was conducted for four stations: Ain Fares, Sidi Kada, Mascara, and Beniane. It is also noteworthy that this second break or rupture resulted in a deficit ranging from –31 to –41%, which is indicative of an escalating trend towards drought.

In light of the findings, it can be posited that the observation series used in this study is predominantly arid, with the exception of the sub-period spanning from 1999 to 2013, which is characterized by elevated precipitation within the prevailing climatic regime in the region.

It is important to note that the majority of previous studies on this subject (Farah, 2013; Dahmani et al., 2024) suggest that this wet period has a significant impact on all rainfall stations in northern Algeria.

In summary, the break detection tests revealed two main phases: a wet period between 1999 and 2006, followed by a break from 2013 to 2014 until the end of the observation series, marked by a significant rainfall deficit (–31 to –41%). Overall, the series remains entirely dry, with only a temporary wet interval (1999-2013).

6.5 Hydrodynamic response of alluvial groundwater

The study of water table fluctuations was conducted to improve our understanding of how the water table reacts to wet climatic conditions. To successfully carry out this study, the SPIs obtained for each sub-period were used, along with the corresponding fluctuating volumes (Fig. 13). The representativeness of water table fluctuations must consider the average piezometric level over 12 months and for each sub-period (SPI). Unfortunately, the required data are unavailable in this case. Furthermore, high water piezometric levels were adopted in the middle of several sub-periods (SPI): 1977, 1983-1993, 1998, 1993-2003, 2007, 2003-2013, 2018, and 2013-2023.

This approach appears to yield conclusive results because the sub-periods used for the water table fluctuation study are identical to those adopted for the SPI. Figure 13 shows the general trend in the temporal evolution of fluctuating water table volumes in relation to climatic humidity. It shows that the temporal evolution of the fluctuating water table volumes and that of climatic humidity are in good agreement. Indeed, the observed volume fluctuations indicate increasingly significant overexploitation of the aquifer. These fluctuations reached –3.973 and –23.644 km^3, respectively, during the drought decades of 1983-1993 and 1993-2003, with an estimated decreasing gradient of –19.67. However, over the last two decades (2003-2013 and 2013-2023),

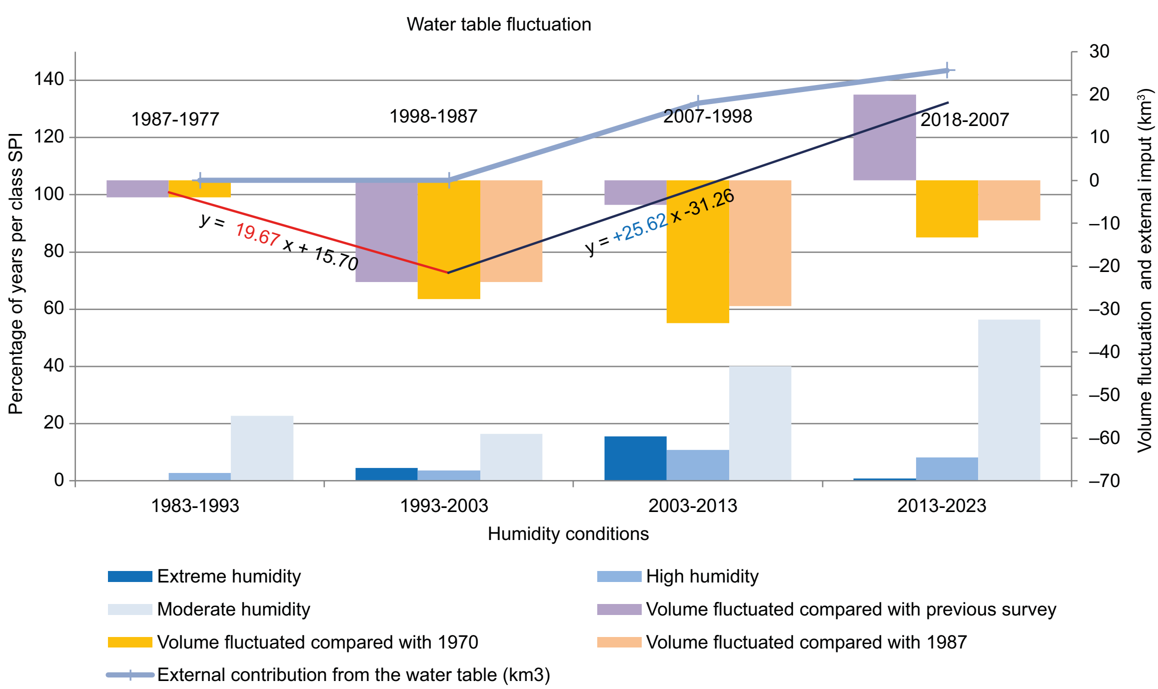

Fig. 13. Temporal evolution of climatic wetness simultaneously with the fluctuating volume and external water table input (1983-2023).

the abundance of rainfall has significantly and progressively contributed to the groundwater recharge, resulting in a volume increase of 17.997 and 25.615 km^3, respectively. This has resulted in relatively positive water balances of –5.647 and +19.968 km^3, with an increasing gradient of +25.62 (see Fig. 13 and Table SIII).

Based on the results obtained, it can be concluded that, despite significant rainfall over the past two decades, the aquifer remains overexploited compared to 1977 and 1987 (–13.296 and –9.323 km^3). This is undoubtedly due to the intensive exploitation of the aquifer during the droughts of the 1980s and 1990s.

It should be noted that the aquifer's water balance during the 2013-2023 decade is relatively greater than that of the previous decade.

The spatio-temporal evolution of water table fluctuations shows a progressive drop in the piezometric level during the dry decades. Figure 14 shows that this fluctuation reached –70 m near the Matemore region during the decade 1993-2003, due to the overexploitation of the aquifer and the multiplication of water points after 1993. On the other hand, an increase in the piezometric level has been recorded since 2003. This level reached a first maximum (+50 m) near Matemore during the decade 1993-2003, and a second maximum (+70 m) during the last decade, south of the study area (Fig. 14).

The spatial evolution of the water table fluctuations during the decades 1993-2003 and 2003-2013 allowed asserting that the aquifer in the Matemore region exhibits a hydrodynamic particularity. Indeed, as illustrated in Figure 5, this aquifer responds quickly and readily to drainage and recharge due to its physical parameters, such as porosity and transmissivity. Furthermore, the significant rise in the water table level observed in the south towards the end of the observation series can be explained by an adjacent recharge resource coming from the continental Pliocene water table when the overflow trigger point is reached.

Generally speaking, the spatial distribution of the water table fluctuation, during the entire observation period between 1983 and 2023, is in good agreement with that of the drawdown (Fig. 5). Indeed, places with lower drawdown (high transmissivity) exhibit an increase in the piezometric level that can reach 30 m near Matemore and to the south of the study area. On the other hand, for places characterized by significant drawdowns, the piezometric level is quite low; it can reach –50 m near Tizi, a small town in the Wilaya of Mascara. In addition, remarkable stability of the piezometric level (between 0 and 10 m) was observed at the outlet; this is generally due to the hydraulic gradient converging towards this zone (Fig. 4).

The above findings indicate that the average fluctuation recorded during the study period results in a negative water balance and, therefore, a deficit volume of –9.323 km3.

In summary, piezometric fluctuations broadly follow the SPI trend, with a marked deficit during the dry decades (1983-2003) and significant recharge after 2003. The Matemore region shows high sensitivity to drainage and recharge phases, in line with its hydrodynamic parameters.

In summary, piezometric fluctuations broadly follow the SPI trend, with a marked deficit during the dry decades (1983-2003) and significant recharge after 2003. The Matemore region shows high sensitivity to drainage and recharge phases, in line with its hydrodynamic parameters.

6.6 Impact of climate variability on land use

A diachronic analysis was conducted across the wet and dry periods to study the impact of the temporal evolution of climatic conditions on land use. In this perspective, the analysis of the spatiotemporal evolution of the different land use classes retained for this study confirmed the expansion of buildings, agriculture and open forest to the detriment of bare soil and dense forest (Table VIII and Fig. 15). Indeed, it turned out that this evolution is the direct consequence of a strategy that had been adopted by the public authorities through a number of intensive agricultural production programs such as the National Agricultural Development Plan (PNDA) and the National Fund for the Development of Agricultural Investment (FNDIA). This operation marked the beginning of intensive irrigated agriculture in 2000. The policy adopted at that time encouraged farmers to convert to market gardening and arboriculture, leading to an increase in agricultural area at the expense of bare soil.

The temporal evolution of the land cover map shows that the study region has undergone significant changes, which are generally linked to climate variability. Indeed, the land use classification of the

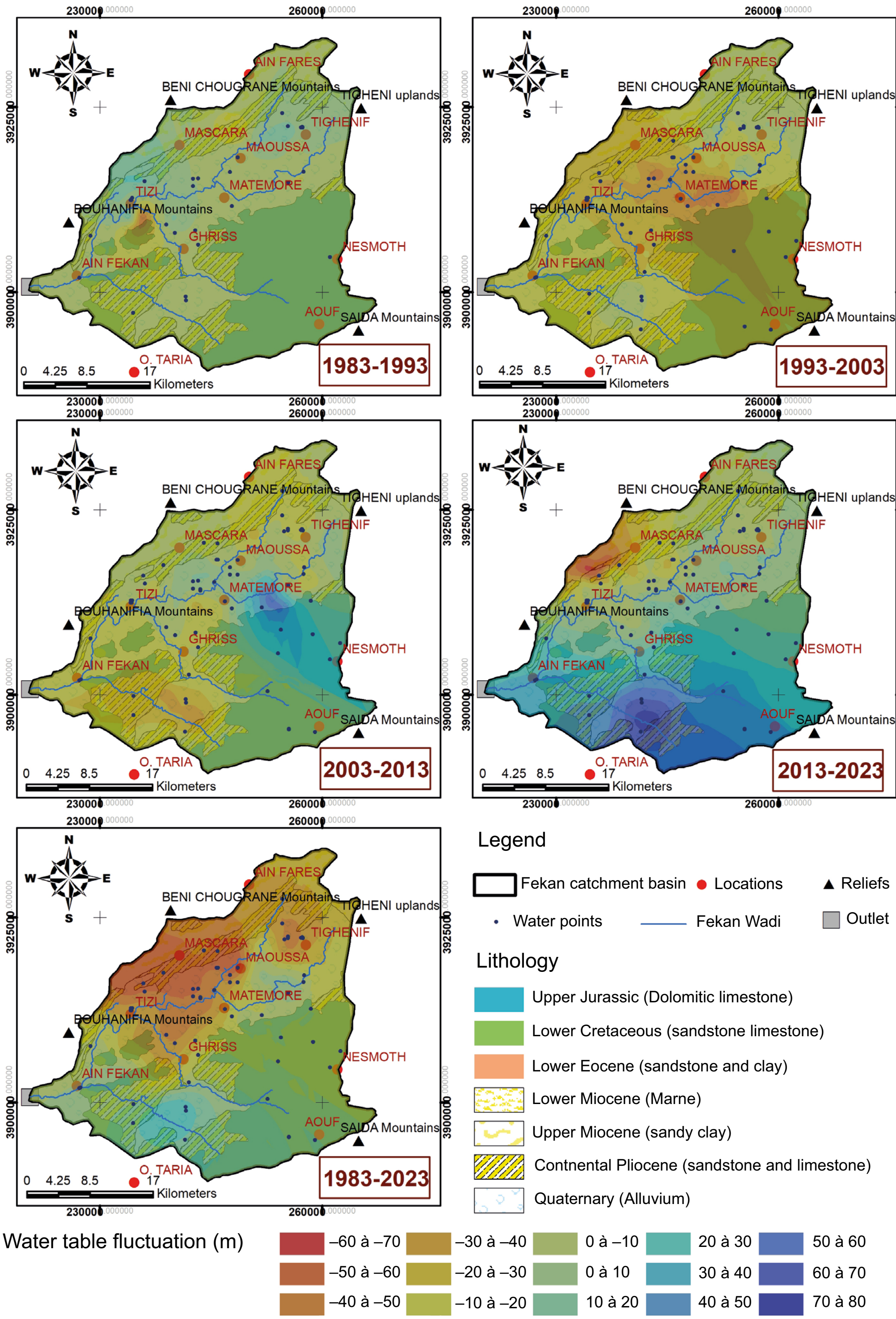

Fig. 14. Spatiotemporal evolution of the water table fluctuation.

Table VIII. Summary of results obtained from supervised classification

Classes	Area (km^2)		Difference (Km^2)	Area (%)		Difference (%)
	1987	2018		1987	2018	
Buildings	14.3	17.57	+3.27	2.99	3.68	+ 0.69
Wadi (river)	0.17	0.39	0.22	0.035	0.08	+0.045
Course	71.76	71.76	0.00	15.01	15.01	0.00
Clear forest	0.12	0.23	+0.11	0.025	0.048	+0.023
Dense forest	0.11	0.1	–0.01	0.023	0.021	–0.002
Bare Soil	51.8	20.84	–30.96	10.84	4.36	–6.48
Agriculture	339.42	367.05	+27.63	71.05	76.80	+5.75

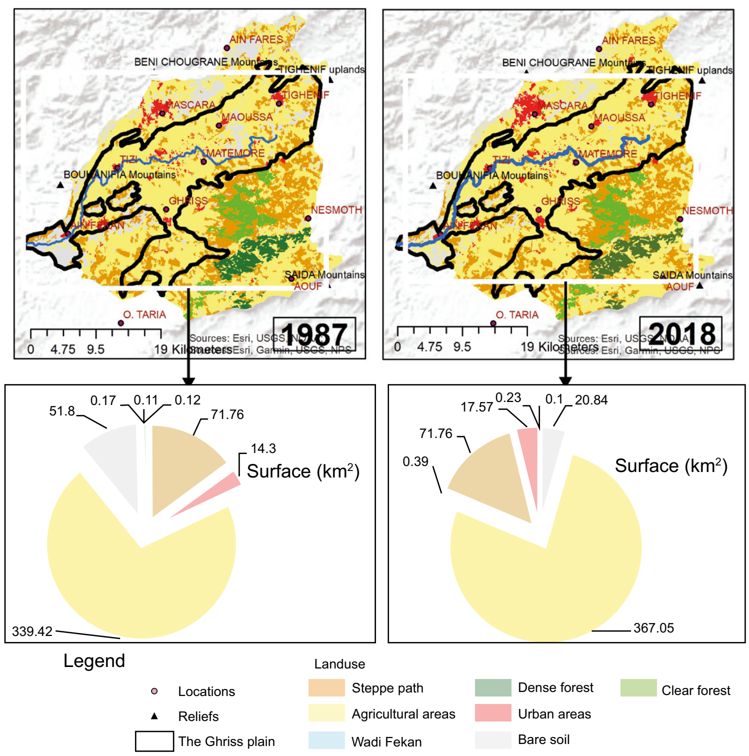

Fig. 15. Spatiotemporal evolution of land use between 1987 and 2018, during high water periods.

Wadi bed has improved over time, particularly in 2018, while the main riverbed has widened. These findings confirm the results of the SPI and CMI, as well as the break detection tests, which indicated excessive rainfall during the period 2013-2023. This rainfall excess can reach almost one quarter of the annual module (24%) calculated during the decade 1983-1993.

The results obtained allow concluding that the temporal evolution of climatic conditions has a significant impact on land use in the study region.

In summary, climate variability has profoundly altered land use, marked by the expansion of the main riverbed. These changes, accentuated by recent excessive rainfall, confirm the direct impact of climate fluctuations on soil dynamics in the study area.

7. Conclusion

The study area, located in the northwestern region of Algeria within the Wadi Fekan watershed and including the Ghriss plain, is an agricultural zone particularly vulnerable to drought. This work aimed to support the sustainable management of groundwater resources and to promote strategies that enhance agricultural resilience and address water scarcity.

Based on a 40-year dataset (1983-2023) from 11 uniformly distributed rainfall stations, the analysis employed drought indices (SPI and CMI), rainfall excess/deficit analysis, and spatiotemporal representations, complemented by break detection tests. The results were validated through an assessment of groundwater fluctuations and land use changes in the basin.

The SPI analysis revealed that 54.5% of years were classified as experiencing drought, with 14.5% corresponding to severe or extreme droughts, particularly during the drought-dominated period of 1983-2003. In contrast, the period from 2003 to 2023 showed an improvement in wetness levels, with notably high values of moderate (40%), high (10.9%), and extreme wet conditions (15.5%) during 2003-2013. The CMI results confirmed this trend, showing a transition from an arid regime (88.2-78.2%) during the first two decades to a semi-arid regime after 2003. However, no fully humid climatic conditions (CMI > 0) were recorded during the entire study period.

Break detection tests identified a major climate shift between 1999 and 2006, consistent with the evolution of the indices. In parallel, the alluvial aquifer showed significant overexploitation during the dry decades (e.g., a deficit of –23.644 km^3 in 1993-2003), with a partial recovery in the wetter period that followed, though the overall water balance remained negative. Between 1987 and 2018, changes in land use show a 5.75% increase in agricultural land and a 0.045% increase in water areas (River), a 6.48% decrease in bare land, and a slight increase in Buildings areas (0.69%). This growing agricultural dynamic is putting greater pressure on water resources, due to increased irrigation requirements and potentially reduced infiltration.

To address the ongoing water deficit, authorities are encouraged to implement sustainable water strategies, including water-saving agricultural practices (e.g., drip irrigation, mulching), responsible water pricing, leak repairs, and restrictions on non-essential water use.

It is important to note that this analysis was conducted at a monthly temporal scale and a regional spatial scale. While this choice effectively captured broad trends in climate variability and its impacts, finer-scale data—such as daily precipitation records or high-resolution spatial imagery (e.g., 10 m or finer)—could reveal localized dynamics and extreme events that the current scale cannot detect. For instance, flash droughts or microclimatic effects are often obscured in coarse-scale analysis. Future studies using higher-resolution temporal and spatial data could offer deeper insight into localized impacts on land use and groundwater recharge.

Finally, a key limitation of this study is the absence of frequency-domain analysis of the climatic time series. Future research should incorporate wavelet transform analysis to identify dominant precipitation and moisture cycles (e.g., annual and decadal) and to investigate multiscale interactions between climate variability and hydrological responses. This method is particularly well-suited to analyze non-stationary climatic signals and would provide a more refined understanding of long-term hydroclimatic dynamics in the region.

Acknowledgments

Thanks are addressed to the Algerian Space Agency, the Integrated Water Resources Management Agency, and the National Hydraulic Resources Agency for providing the data required for this study.

References

Aicha EM, Naouel B, Meddi M. 2011. Contribution à l'étude du changement climatique du bassin versant de l'oued El Hammam (Nord-Ouest d'Algérie). In: Conference: ICCAFFE 2011: Climate change, agri-food, fisheries, and ecosystem. Reinventing research, innovation and policy agendas, environmentally and socially-balanced growth. Agadir, Morocco. https://doi.org/10.13140/2.1.1615.1841

Amiar S, Bouanani A, Baba-Hamed K, Belarbi H. 2020. Variabilité pluviométrique dans le bassin versant du Haut et Moyen Cheliff. Revue des Sciences de l'Eau/ ournal of Water Science 32: 337-347. https://doi.org/10.7202/1069569ar

Ardoin S, Lubes-Niel H, Servat E, Dezetter A, Boyer J-F, Mahe G, Paturel J-E. 2003. Analyse de la persistance de la sécheresse en Afrique de l'ouest: caractérisation de la situation de la décennie 1990. Hydrology of the Mediterranean and Semiarid Regions (proceedings of an international symposium held at Montpellier). IAHS Publication 278: 223-228.

Baba-Hamed K, Bouanani A, Nasri A, Bouanani R. 2015. La modelisation de la nappe alluviale de la Plaine de Ghriss (mascara Nw-Algerien). LARHYSS Journal 12: 133-140.

Beaulieu C, Seidou O, Ouarda TBMJ, Zhang X, Boulet G, Yagouti A. 2008. Intercomparison of homogenization techniques for precipitation data. Water Resources Research 44: 1-20. https://doi.org/10.1029/2006WR005615

Beaulieu C. 2009. Homogénéisation des séries de précipitations: identification des techniques les plus prometteuses et nouveaux développements. Institut National de la Recherche Scientifique, Université du Québec.

Bekkoussa SM. 2020. Approche hydrogéologique et hydrochimique des echanges entre aquifères profonds et superficiels du bassin d'Oued Fekan. Ph.D. thesis. Université Mustapha Stambouli, Mascara.

Bessedik M, Abdelbaki C, Tiar SM, Badraoui A, Megnounif A, Goosen M, Mourad KA, Baig MB, Alataway A. 2023. Strategic decision-making in sustainable water management using demand analysis and the water evaluation and planning model. Sustainability 15: 16083. https://doi.org/10.3390/su152216083

Bodian A. 2014. Caractérisation de la variabilité temporelle récente des précipitations annuelles au Sénégal (Afrique de l'Ouest). Physio-Géo 8: 297-312. https://doi.org/10.4000/physio-geo.4243

Bois P. 1971. Une méthode de contrôle de séries chronologiques utilisées en climatologie et en hydrologie. Publication du Laboratoire de Mécanique des Fluides, Section Hydrologie, Université de Grenoble.

Bougara H, Hamed KB, Borgemeister C, Tischbein B, Kumar N. 2021. A comparative assessment of meteorological drought in the Tafna basin, northwestern Algeria. Journal of Water and Land Development 51: 78-93. https://doi.org/10.24425/jwld.2021.139018

Boyer JF. 2002. Logiciel Khronostat d'analyse statistique de séries chronologique/Software Khronostat chronological series of statistical analysis. IRD UR2, Program 21 Friend AOC, Team UMRGBE Hydrology, University of Montpellier II, Ecole des Mines de Paris.

Brunet-Morel Y. 1977. Test d'homogénéité. Cahiers Orstom, Série Hydrologie 14: 119-128.

Buishand TA. 1982. Some methods for testing the homogeneity of rainfall records. Journal of Hydrology 58: 11-27. https://doi.org/10.1016/0022-1694(82)90066-X

Cohen J. 1960. A coefficient of agreement for nominal scales. Educational and Psychological Measurement 20: 37-46. https://doi.org/10.1177/001316446002000104

CSEN. 2022. Glossaire à l'usage des équipes éducatives et des éco-délégués (Guilyardi E, Ed.). Conseil Scientifique de l'Éducation Nationale.

Dagnelie P. 1970. Théorie et méthodes statistiques. 2. Les méthodes de l'inférence statistique: applications agronomiques. J. Duculot, Gembloux.

Dahmani MN, Baba-Hamed K, Bouanani A. 2024. Assessing the consequences of climate variability in the Wadi Saida watershed, northwestern Algeria. Water Practice & Technology 19: 987-1002. https://doi.org/10.2166/wpt.2024.058

Dao A, Kamagate B, Mariko A, Goula BTA, Seguis L, Bokar MH, Savane I. 2010. Variabilité climatique et réponse hydrologique du bassin versant transfrontalier de Kolondièba au Sud du Mali. European Journal of Scientific Research 43: 435-444.

Djellouli F. 2017. Persistance de la variabilité climatique et occurrence de la sécheresse: La modélisation « pluie-débit » outil d'identification. Application à un bassin versant d'oued El Hammam (Nord-ouest algérien). Ph.D. thesis. Université de Tlemcen, Abou Bekr Belkaid.

Eriksen SH, Kelly PM. 2007. Developing credible vulnerability indicators for climate adaptation policy assessment. Mitigation and Adaptation Strategies for Global Change 12: 495-524. https://doi.org/10.1007/s11027-006-3460-6

Farah AK. 2013. Changement climatique ou variabilité climatique dans l'Est algérien. M.Sc. thesis. Université Frères Mentouri Constantine 1.

Faty A, Kane A, Ndiaye AL. 2017. Influence de la manifestation climatique sur les régimes pluviométriques saisonniers dans le haut bassin versant du Sénégal/Influence of climate on seasonal rainfall patterns in the upper watershed of Senegal. Revue des Sciences de l'Eau/Journal of Water Science 30: 79-87. https://doi.org/10.7202/1042915ar

Faye C, Sow AA, Ndong JB. 2015. Étude des sècheresses pluviométriques et hydrologiques en Afrique tropicale: caractérisation et cartographie de la sècheresse par indices dans le haut bassin du fleuve Sénégal. Géographie Physique et Environnement 9: 17-35. https://doi.org/10.4000/physio-geo.4388

GeoRGB Community. 2023. Ordinary kriging 5-step practical guide. Available at: https://giscourse.online/ordinary-kriging-5-step-practical-guide/ (accessed on June 7, 2025).

Ghenim AN. 2013. Détection de la sécheresse pluviométrique dans le bassin de la Tafna au cours des six dernières décennies. Communication Science et Technologie 11: 26-31.

Gherissi R. 2018. Modélisation hydrologique d'un bassin versant en climat méditerranéen par l'approche conceptuelle globale. Cas de l'oued Lakhdar (ex: Chouly) (Tafna, Nord-Ouest algérien). Ph.D. thesis. Université de Tlemcen-Abou Bekr Belkaid.

Giddings L, Soto M, Rutherford BM, Maarouf A. 2005. Standardized precipitation index zones for Mexico. Atmósfera 18: 33-56.

Goula AM, Adamopoulos KG. 2005. Spray drying of tomato pulp in dehumidified air: II. The effect on powder properties. Journal of Food Engineering 66: 35-42. https://doi.org/10.1016/j.jfoodeng.2004.02.031

Gratton Y. 2002. Le krigeage: la méthode optimale d'interpolation spatiale. L'Institut D'Analyse Géographique 1, Québec.

Hallouz F, Meddi M, Mahé G. 2012. Etude des relations pluie/debit via les coefficients d'ecoulement et le cumul de deficit de pluie dans le bassin versant de l'Oued Mina (nord ouest d'Algerie)/Study of the rainfall/runoff relationships through runoff coefficients and sum of rainfall deficit in the bassin of the Wadi Mina (northwest of Algeria). Le Journal de l'Eau et de l'Environnement 11: 37-47.

Hubert P, Carbonnel JP, Chaouche A. 1989. Segmentation des séries hydro-météorologiques: application à des séries des précipitations et de débits de l'Afrique de l'ouest. Journal of Hydrologie 110: 349-367. https://doi.org/10.1016/0022-1694(89)90197-2

Hubert P. 2000. The segmentation procedure as a tool for discrete modeling of hydrometeorological regimes. Stochastic Environmental Research and Risk Assessment 14: 297-304. https://doi.org/10.1007/PL00013450

IPCC. 2007. Climate change 2007. Synthesis report. Contribution of working groups I, II and III to the Fourth Assessment Report of the Intergovernmental Panel on Climate Change (Core Writing Team, Pachauri R.K and Reisinger A., Eds.). Intergovernmental Panel on Climate Change, Geneva, Switzerland, 104 pp.

Issartel J. 2007. Adaptation de la faune souterraine aux basses températures: mécanismes et enjeux écologiques. Ph.D. thesis. Université Claude Bernard-Lyon I.

Jaziri B, Samaali H, Mjejra M. 2019. L'apport des indices SPI et NDVI pour l'évaluation des conditions du risque de secheresse aux alentours du Barrage Sejnane (Tunisie septentrionale). Annals of the University of Bucharest: Geography Series LXVII.

Jouilil I, Bitar K, Salama H, Amraoui A, Mokssit A, Tahiri M. 2013. Sécheresse météorologique au bassin hydraulique OUM ER RBIA durant les dernières décennies. LARHYSS Journal 10: 109-127.

Kartoubi M, Hartani T, Hallouze F. 2017. Impact de changement climatique sur les ressources en eau dans la plaine de Khemis Miliana (bassin versant du Haut Cheliff). Systèmes Agraires et Environnement 1: 40-48.

Khoualdia W, Djebbar Y, Hammar Y. 2014. Caractérisation de la variabilité climatique: cas du bassin versant de La Medjerda (nord-est Algérien)/Characterization of climate variability: Case of watershed medjerda (north-east of Algeria). Synthèse: Revue des Sciences et de la Technologie 20: 6-23.

Kingumbi A, Bergaoui Z, Bourges-Jacques HP, Kallel R. 2001. Étude de l'évolution des séries pluviométriques en Tunisie centrale. In: Séminaire International Montpellier 2000 Hydrologie des Régions Méditerranéennes (Servat E, Albergel J, Eds.). UNESCO, Montpellier, 341-350. (Documents Techniques en Hydrologie, 51).

Laborde J. 2007. Geographical information and climatology for hydrology. In: Geographical information and climatology (Carrega P, Ed.). John Wiley & Sons, London and Hoboken, 195-232.

Lamb PJ. 1982. Persistance of Subsaharan drought. Nature: 299. 46-47. https://doi.org/10.1038/299046a0

Lee AFS, Heghinian SM. 1977. A shift of the mean level in a sequence of independent normal random variables—A Bayesian approach—. Technometrics 19: 503-506. https://doi.org/10.1080/00401706.1977.10489592

Lubès H, Masson JM, Servat E, Paturel J-E, Kouame B, Boyer J-F. 1994. ICCARE: rapport no. 3: caractérisation de fluctuations dans une série chronologique par applications de tests statistiques: étude bibliographique. ORSTOM, Montpellier, 22 pp.

Lubes-Niel H, Masson JM, Paturel JE, Servat E. 1998. Variabilité climatique et statistiques. Étude par simulation de la puissance et de la robustesse de quelques tests utilisés pour vérifier l'homogénéité de chroniques. Revue des Sciences de L'eau 11: 383-408. https://doi.org/10.7202/705313ar

Mahcer I, Baahmed D, Oudin L, Chemirik CHK. 2024. Multidimensional analysis of NDVI dynamics in response to climate and land use/land cover change in northwest Algeria. Journal of Hydrology and Hydromechanics 72: 399-412. https://doi.org/10.2478/johh-2024-0020

Mahé G, Olivry J-C. 1995. Variations des précipitations et des écoulements en Afrique de l'Ouest et Centrale de 1951 à 1989. Sécheresse 6: 109-117.

McKee TB, Doesken NJ, Kleist J. 1993. The relation of drought frequency and duration to time scales. In: Proceedings of the 8th Conference on Applied Climatology, Anaheim, 179-184.

Milano M. 2010. Les impacts prévisibles du changement climatique sur les ressources en eau de quatre grands bassins versants méditerranéens. Available at: https://planbleu.org/wp-content/uploads/2010/01/impact_cc_eau_fr.pdf (accessed on November 18, 2025).

Niang AJ, Ozer A, Ozer P. 2008. Fifty years of landscape evolution in southwestern Mauritania by means of aerial photos. Journal of Arid Environments 72: 97-107. https://doi.org/10.1016/j.jaridenv.2007.04.009

Nur'eni, Jamidun, Setiawan I, Suaib NM. 2020. Estimation of ordinary kriging parameters for determining characteristics and distribution of groundwater layer in Tondo area, Mantikulore district, Palu. Journal of Physics: Conference Series 1434: 012025. https://doi.org/10.1088/1742-6596/1434/1/012025

Otmane A, Baba-Hamed K, Bouanani A, Kebir LW. 2018. Mise en évidence de la sécheresse par l'étude de la variabilité climatique dans le bassin versant de l'oued Mekerra (nord-ouest algérien). Techniques, Sciences, Méthodes: 23-37. https://doi.org/10.1051/tsm/201809023

Paturel JE, Servat E, Delattre MO, Lubes-Niel H. 1998. Analyse de séries pluviométriques de longue durée en Afrique de l'Ouest et Centrale non sahélienne dans un contexte de variabilité climatique. Hydrological Sciences Journal: 43. 937-946. https://doi.org/10.1080/02626669809492188

Pettitt AN. 1979. A Non-parametric approach to the change-point problem. Journal of the Royal Statistical Society, Series C (Applied Statistics): 28. 126-135. https://doi.org/10.2307/2346729

Potere D. 2008. Horizontal positional accuracy of Google Earth's High-resolution imagery archive. Sensors 8: 7973-7981. https://doi.org/10.3390/s8127973

Richards JA, Jia X. 2006. Remote sensing digital image analysis: An introduction. Springer, Berlin, Heidelberg. https://doi.org/10.1007/3-540-29711-1

Sonmez S, Kirilmaz L, Yucesoy M, Yücel B, Yilmaz B. 2005. The effect of bee propolis on oral pathogens and human gingival fibroblasts. Journal of Ethnopharmacology 102: 371-376. https://doi.org/10.1016/j.jep.2005.06.035

Soro GE, Anouma DGL, Goula BTA, Srahorou B, Savané I. 2014. Caracterisation des sequences de secheresse méteorologique a diverses echelles de temps en climat de type soudanais: cas de l'extreme nord-ouest de la Cote d'Ivoire. Larhyss Journal: 18. 107-124.

Turc L. 1954. Le bilan d'eau des sols. Relation entre la précipitation, l'évaporation et l'écoulement. In: Pluie, évaporation, filtration et écoulement. Compte rendu des troisièmes journées de l'hydraulique. Algeria, April 12-14, 36-44.

Vörösmarty CJ, Douglas EM, Green PA, Revenga C. 2005. Geospatial Indicators of emerging water stress: An application to Africa. AMBIO: A Journal of the Human Environment 34: 230-236. https://doi.org/10.1579/0044-7447-34.3.230

Willmott CJ, Feddema JJ. 1992. A more rational climatic moisture index. The Professional Geographer 44: 84-88. https://doi.org/10.1111/j.0033-0124.1992.00084.x

Wu H, Hayes MJ, Weiss A, Hu Q. 2001. An evaluation of the Standardized Precipitation Index, the China-Z Index and the statistical Z-Score. International Journal of Climatology 21: 745-758. https://doi.org/10.1002/joc.658

Supplementary material

Table SI. Hydrodynamic data from the selected water points.

Number	Name	Coordinates (in decimal degrees)		Depth (m)	Static level	Dynamic level	Reduction
		X	Y				
1	G2 Aeroport	269100	214700	250	43.6	67.2	23.60
2	E2Mascara	270000	231100	200	9.0	43.3	34.30
3	E20 Ghriss	270350	224150	265	17.5	35.3	17.89
4	E3 Mascara	270000	230100	400	4.0	88.6	84.55
5	E42 Ghriss	269500	218500	342	66.0	86.0	20.00
6	E5 Mascara	270700	231150	400	4.7	50.5	45.76
7	E8 Mascara	263500	230750	273	10.4	115.8	105.40
8	E44 Mascara	271000	230000	512	65.0	76.0	11.00
9	E45 Mascara	271000	229850	396	60.8	76.0	15.23
10	E30 Industrielle	266000	233280	200	51.9	88.7	36.80
11	E28 Selatna	271450	236300	250	35.5	95.3	59.80
12	E22 Tizi	261800	228500	243	15.5	48.1	32.62
13	E29 Tizi	261650	228500	250	18.0	45.0	27.00
14	E40 Tizi	272900	231000	276	51.6	57.0	5.40
15	E27 El Keurt	263300	231850	250	32.5	80.8	48.25
16	S1 Tighennif	284700	238150	150	1.9	31.8	29.90
17	S2 Tighennif	284550	238050	86	12.0	45.0	33.00
18	S3 Tighennif	284750	238050	82	3.0	40.0	37.00
19	E1 Tighennif	282800	238200	100	18.0	54.0	36.00
20	E24 Tighennif	282000	240000	166	36.2	73.2	37.00
21	E32 O/Khamsa	282300	237850	115	13.3	59.0	45.70
22	E33 Tighennif	282800	238000	100	20.4	56.5	36.10
23	E41 Tighennif	285000	233000	450	65.0	71.0	6.00
24	S1 Tighennif	284800	238000	80	6.0	68.0	62.00
25	E12 Sidi Kada	282850	230620	253	20.0	31.6	11.60
26	E25	279300	227600	250	32.6	51.6	19.05
27	E26 Sidi Salem	282750	230600	164	31.1	52.4	21.30
28	Sidi Kada	285900	228500	120	17.0	20.0	3.00
29	NE1 Nesmoth	288500	220600	250	58.3	80.1	21.80
30	NE2 Nesmoth	289900	222800	200	27.2	65.6	38.40
31	E23 Sidi Kada	284900	232100	225	18.9	59.0	40.11
32	B.A.N Ghriss	269050	215200	300	30.0	86.0	56.00
33	E13 Ghriss	270700	222200	310	22.5	42.5	20.00
34	E10 Matemore	275280	227430	250	18.2	51.0	32.80
35	E31 Matemore	274300	228400	170	28.2	60.0	31.80
36	E14 Froha	266400	224900	300	28.3	75.5	47.20
37	E17 Maoussa	275000	232000	200	13.5	57.2	43.70
38	E18 Maoussa	276000	234000	230	22.3	26.4	4.10
39	E43 Maoussa	276000	232000	224	30.0	48.0	18.00
40	S/Ben Yekhlef	273300	236200	250	42.0	98.0	56.00
41	E37 Karrech	275000	233000	250	41.0	71.0	30.00
42	E38 S/B Yekhlef	273350	234000	266	49.0	80.0	31.00
43	E21 Ain Fekan	254700	217700	100	17.0	42.6	25.60
44	E36 Ain Fekan	254900	217800	200	28.0	91.0	63.00
45	OT5 O/Taria	269000	210800	170	22.0	83.0	61.00
46	G1 Guerdjoum	262000	213000	280	13.5	52.0	38.50
47	G3 Guerdjoum	262000	215600	205	45.0	80.0	35.00
48	MA2 S/M'Barak	286500	210800	150	14.3	71.2	56.90
49	Makda 1 Makda	283000	211200	132	10.2	39.1	28.88
50	IW Maoussa	273200	234000	242	26.0	78.0	52.00
51	SK2 S/Boussaid	281900	224600	250	6.8	62.0	55.20

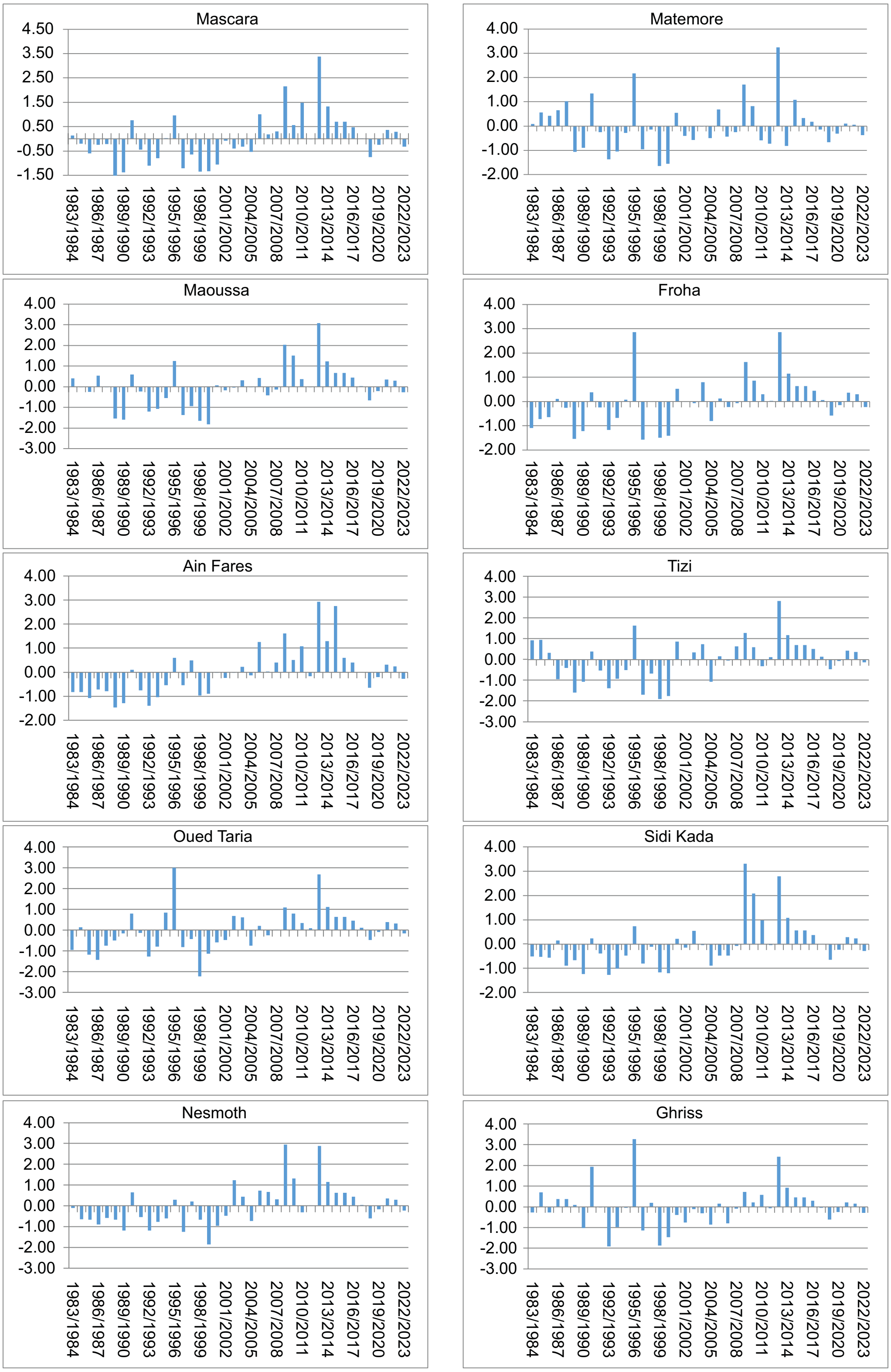

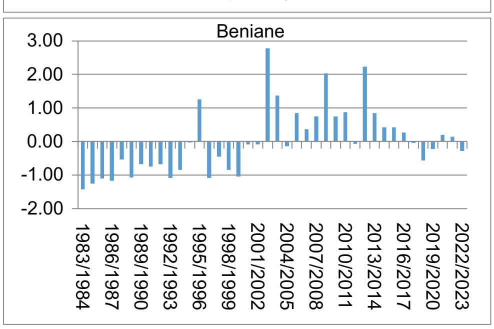

Fig. S1. Temporal evolution of SPI values for the different stations selected (1983/84-2022/23)

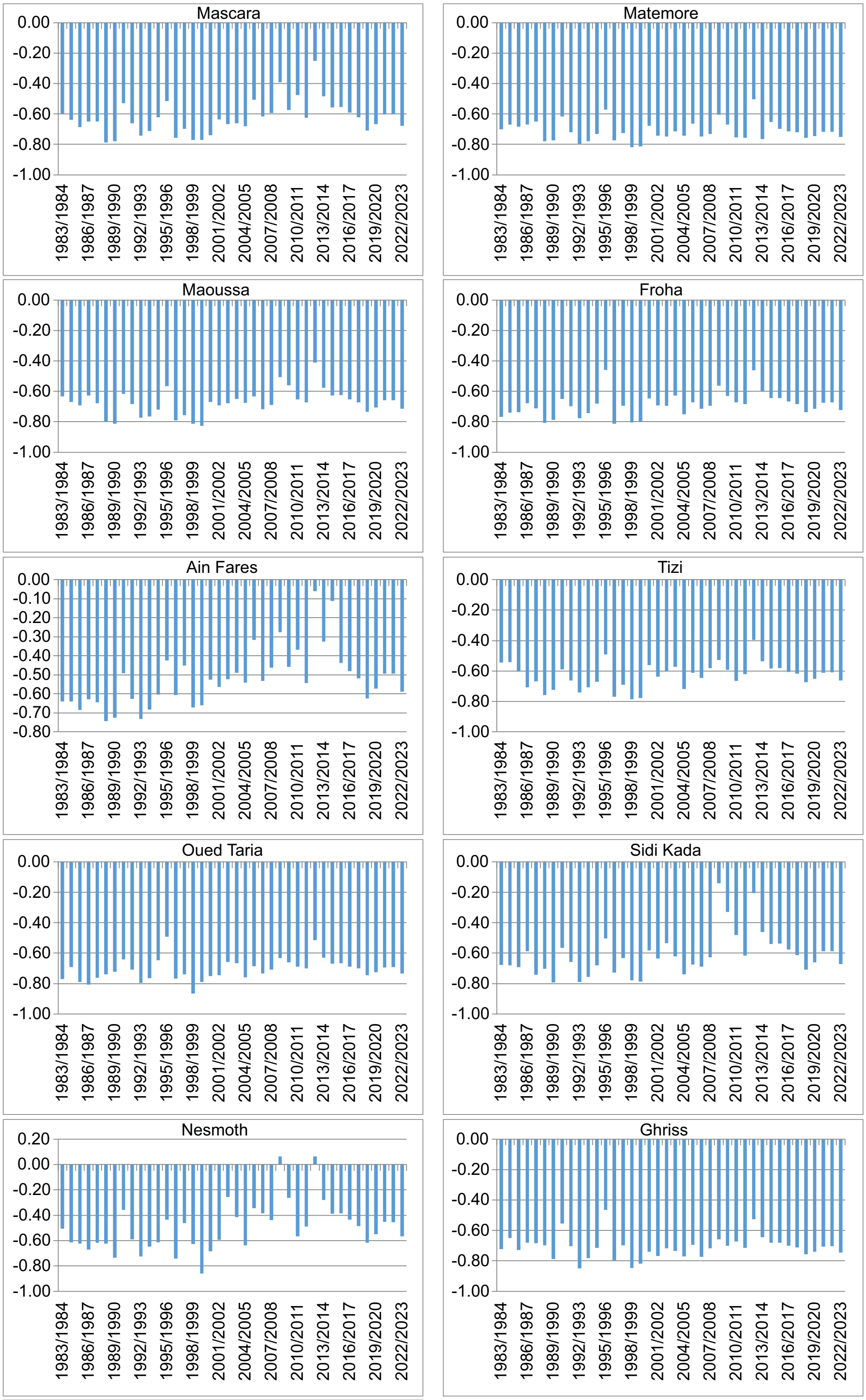

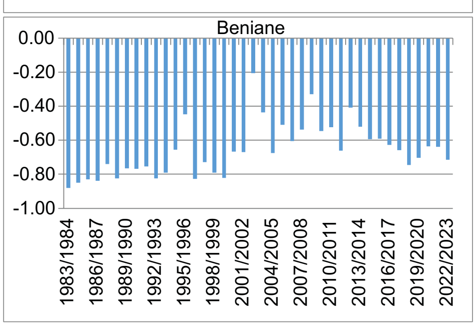

Fig.S2. Temporal evolution of the CMI values for the different stations selected (1983/84-2022/23)

Table SII. Results of the break detection tests applied to rainfall data between 1983 and 2023.

Table SII. Results of the break detection tests applied to rainfall data between 1983 and 2023.

Station	Break (rupture) test	Year/ period of break	Average before 1 break	Average after 1 break	Average after 2 breaks	Average after 3 breaks	Deficit and excess (%)
Ghriss	Lee and Heghinian						
	Pettitt	2007	264.352	303.617			14.9
	Segmentation Hubert	[1983-2023]		279.082			
Matemore	Lee and Heghinian	1987	309.420	271.215			–12.3
	Pettitt						
	Segmentation Hubert	[1983-2023]		275.988			
Maoussa	Lee and Heghinian						
	Pettitt	2002					
	Segmentation Hubert	[1983-2008] [2008-2023]	281.636	363.193			29.0
Froha	Lee and Heghinian	1999	260.553	327.039			25.5
	Pettitt	1999	260.553	327.039			25.5
	Segmentation Hubert	[1983-2000] [2000-2023]	260.553	327.039			25.5
Ain Fares	Lee and Heghinian	2001	364.921	546.491			49.8
	Pettitt	2001	364.921	546.491			49.8
	Segmentation Hubert	[1983-2002] [2002-2012] [2012-2015] [2015-2023]	364.921	531.000	806.533	468.338	45.5 51.9 **–41.9**
Tizi	Lee and Heghinian	1999	312.529	387.204			23.9
	Pettitt	1999	312.529	387.204			23.9
	Segmentation Hubert	[1983-2000] [2000-2023]	312.529	387.204			23.9
Oued Taria	Lee and Heghinian	2001	252.668	309.027			22.3
	Pettitt	2001	252.668	309.027			22.3
	Segmentation Hubert	[1983-1995] [1996-2002] [2002-2023]	251.058	217.000	309.038		–13.6 42.4
Sidi kada	Lee and Heghinian	2007	312.300	475.120			52.1
	Pettitt	2006	310.242	468.031			50.9
	Segmentation Hubert	[1983-2008] [2008-2014] [2014-2023]	312.300	608.383	386.278		94.8 **–36.5**
Nesmoth	Lee and Heghinian	2001	365.668	590.533			61.5
	Pettitt	2001	365.668	590.533			61.5
	Segmentation Hubert	[1983-2002] [2002-2023]	365.668	590.533			61.5
Mascara	Lee and Heghinian	2004	306.300	428.868			40.0
	Pettitt	2004	306.300	428.868			40.0
	Segmentation Hubert	[1983-2004] [2004-2012] [2013-2023]	306.343	428.537	388.230		39.9 **–9.4**
Beniane	Lee and Heghinian	1999	216.982	418.654			92.9
	Pettitt	2001	227.800	428.073			87.9
	Segmentation Hubert	[1983-2002] [2002-2014] [2014-2023]	227.800	495.175	338.611		117.4 **–31.6**
Average excess							36.41%

Table SIII. Assessment of fluctuations in groundwater volume for different periods and estimation of external water inputs during the wet period.

Fluctuation height		1987-1970		1998-1987		2007-1998		2018-2007	
Interval (m)	Average	Area (m^2)	Volume (m^3)	Area (m^2)	Volume (m^3)	Area (m^2)	Volume (m^3)	Area (m^2)	Volume (m^3)
–70 to –60	–65							781653	–50807445
–60 to –50	–55			737229	–40547595			7815310	–429842050
–50 to –40	–45	1701330	–76559850	19638600	–883737000			11782600	–530217000
–40 to –30	–35	4499110	–157468850	140016000	–4900560000	12502400	–437584000	14636900	–512291500
–30 to –20	–25	9013231	–225330775	440382000	–11009550000	94881300	–2372032500	24678200	–616955000
–20 to –10	–15	58509900	–877648500	386922000	–5803830000	362674000	–5440110000	47950500	–719257500
–10 to 0	–5	879220000	–4396100000	203609000	–1018045000	431975000	–2159875000	194098000	–970490000
0 to 10	5	187322000	936610000	2459650	12298250	122712000	613560000	235542000	1177710000
10 to 20	15	51350500	770257500			63174300	947614500	137921000	2068815000
20 to 30	25	2130310	53257750			66448900	1661222500	155451000	3886275000
30 to 40	35					26612900	931451500	127288000	4455080000
40 to 50	45					9821300	441958500	118455000	5330475000
50 to 60	55					3033140	166822700	81911900	4505154500
60 to 70	65							28005500	1820357500
70 to 80	75							7392900	554467500
Total volume fluctuated (km^3)		**–3.973**		**–23.644**		**–5.647**		**19.968**	
Externel input (km^3)						**17.997**		**25.615**	
Fluctuation with respect to the year 1970 (km^3)		**–3.973**		**–27.617**		**–33.264**		**–13.296**	
Fluctuation with respect to the year 1987 (km^3)		-		**–23.644**		**–29.291**		**–9.323**	

Table SIV. Kriging parameters.

Parameters	Value
Nugget	0.609628481634
Partial sill	0.477673336278
Range	343.743895402324

Table SV. Confusion matrix for 1987 (accuracy ≈ 90.0 %, kappa ≈ 0.8025).

Real/classified	Agriculture	Bare soil	Built	Light forest	Dense forest	Course	Water	Real total	Producer accuracy (%)
Agriculture	339 649	6 220	6 361	6 297	6 177	6 353	6 331	377 388	90.00
Bare soil	905	51 834	975	964	988	996	932	57 594	90.00
Built	267	261	14 309	259	290	273	240	15 899	90.00
Light forest	0	5	5	119	2	1	1	133	89.47
Dense forest	1	3	2	1	109	3	3	122	89.34
Course	1 270	1 321	1 341	1 384	1 325	71 807	1 338	79 786	90.00
Water	1	2	1	4	5	6	170	189	89.95
Classified total	342 093	59 646	22 994	9 028	8 896	79 439	9 015	531 111	
UA (%)	99.29	86.90	62.23	1.32	1.23	90.39	1.89		

Table SVI. Confusion matrix for 2018 (accuracy ≈ 92.0 %, kappa ≈ 0.839).

Real/classified	Agriculture	Bare soil	Built	Light forest	Dense forest	Course	Water	Real total	Producer accuracy (%)
Agriculture	347 196	4 967	5 072	5 115	4 953	5 156	4 929	377 388	92.00
Bare soil	782	52 986	752	733	805	759	777	57 594	92.00
Built	206	228	14 627	212	214	219	193	15 899	92.00
Light forest	0	0	3	122	2	3	3	133	91.73
Dense forest	3	1	1	2	112	1	2	122	91.80
Course	1 053	1 023	1 061	1 099	1 042	73 403	1 105	79 786	92.00
Water	3	4	4	1	1	3	173	189	91.53
Classified total	349 243	59 209	21 520	7 284	7 129	79 544	7 182	531 111	
UA (%)	99.41	89.49	67.97	1.67	1.57	92.28	2.41		